Frequency-domain modelling of reset control systems using an impulsive description

Buitenhuis, R. N.; Saikumar, N.; HosseinNia, S. Hassan

DOI
10.1016/j.nahs.2023.101341

Publication date
2023

Document Version
Final published version

Published in
Nonlinear Analysis: Hybrid Systems

Nonlinear Analysis: Hybrid Systems 49 (2023) 101341

Contents lists available at ScienceDirect

Nonlinear Analysis: Hybrid Systems

journal homepage: www.elsevier.com/locate/nahs

Frequency-domain modelling of reset control systems using an impulsive description

R.N. Buitenhuis [a,b], N. Saikumar [a], S. Hassan HosseinNia [a,*]

[a] Department of Precision and Micro Systems Engineering, 3ME, Delft University of Technology, The Netherlands
[b] Delft Center for Systems and Control, 3ME, Delft University of Technology, The Netherlands

ARTICLE INFO

Article history:
Received 23 August 2021
Received in revised form 24 January 2023
Accepted 25 February 2023
Available online xxxx

Keywords:
Reset control
Closed-loop
Nonlinear control
Impulsive modelling
Describing function
Frequency domain
Precision control
Mechatronics
Motion control

ABSTRACT

The ever-increasing industry desire for improved performance makes linear controller design run into fundamental limitations. Nonlinear control methods such as Reset Control (RC) are needed to overcome these. RC is a promising candidate since, unlike other nonlinear methods, it easily integrates into the industry-preferred PID design framework. Thus far, RC has been analysed in the frequency domain either through describing function analysis or by direct closed-loop numerical computation. The former computes a simplified closed-loop RC response by assuming a sufficient low-pass behaviour. In doing so it ignores all harmonics, which literature has found to cause significant modelling prediction errors. The latter gives a precise solution, but by its direct closed-loop computation does not clearly show how open-loop RC design translates to closed-loop performance. The main contribution of this work is aimed at overcoming these limitations by considering an alternative approach for modelling RC using state-dependent impulse inputs. This permits accurately computing closed-loop RC behaviour starting from the underlying linear system, improving system understanding. A frequency-domain description for closed-loop RC is obtained, which is solved analytically by using several well-defined assumptions. This analytical solution is verified using a simulated high-precision stage, critically examining sources of modelling errors. The accuracy of the proposed method is further substantiated using controllers designed for various specifications.

1. Introduction

Industry is continuously pushing control limitations by increasing performance demands. This causes requirements on bandwidth, disturbance rejection, noise attenuation and reference tracking to become increasingly stringent. PID and other linear controllers are standard to industry, also to high-tech applications. This status is expected to prevail [1], because these controllers permit the industry preferred loop-shaping design framework. Linear control is inherently subject to fundamental limitations, including the Bode gain-phase relationship [2]. This links bandwidth, disturbance rejection, noise attenuation and reference tracking. One cannot improve on some aspect without compromising on another. This design trade-off hinders the industry push for better performance.

This trade-off can only be overcome through nonlinear control, such as Reset Control (RC). RC is a promising candidate as various implementations embed nicely into PID and additionally the industry preferred loop-shaping framework. The

* Corresponding author.
E-mail addresses: RubenNBuitenhuis@gmail.com (R.N. Buitenhuis), niranjans87@gmail.com (N. Saikumar), S.H.HosseinNiaKani@tudelft.nl (S. Hassan HosseinNia).

https://doi.org/10.1016/j.nahs.2023.101341

first reset element was the Clegg Integrator (CI) [3], which is an integrator with its state value resetting to zero whenever its input crosses zero. Through Describing Function (DF) analysis [4] it is shown that the CI inflicts 52° less phase lag than the in gain similar linear integrator, thus overcoming the Bode gain-phase relationship.

Several authors made contributions towards generalizing the CI. The first extension was by resetting a first-order low-pass filter known as the First Order Reset Element (FORE) [5]. Further developments enhancing design flexibility include second-order [6] and fractional-order [7] reset elements, as well as a second-order single-state reset element [8]. Additional tuning freedom was obtained by allowing states to be reset to non-zero values [9,10]. Recently, the Constant-in-Gain Lead-in-phase (CgLp) RC implementation was proposed [11], designed to provide a broadband phase lead without affecting the gain. This property makes CgLp very suitable to be used in combination with any linear controller.

The reset law accompanying a reset element determines when a reset occurs. Traditionally, that is when the input of the reset element crosses zero [3]. Extensions [12,13] and alternatives [14–19] are mentioned in literature, providing a variety of RC behaviours, tuning possibilities, stability results and performance analysis [20,21]. These options are not considered here, as loop-shaping based RC tuning is developed for zero-crossing reset laws, where the zero-crossing is not restricted to the error signal.

Several works have demonstrated that RC can push performance beyond limits attainable through linear control [22–25], for example by reducing overshoot [26] without affecting other specifications. RCs have been implemented in various control applications, including chemical processes [16], vibration isolation [27] and motion control systems [17,28–31].

A frequency-domain description of RC is imperative for design using the loop-shaping methodology preferred by industry. Most commonly, DF analysis is utilized [10], which ignores all output harmonics. Despite this popularity, several works found DF to yield predictions in closed-loop that deviated widely from measurements [27,32,33]. Recently, an open-loop extension of DF analysis, incorporating harmonics termed higher-order sinusoidal input describing functions (HOSIDFs), was used together with various assumptions to compute a novel closed-loop frequency-domain description, CL-DF [34]. DF assumes the reset element to have a sinusoidal input, while CL-DF assumes that the higher harmonics are small relative to the main harmonic, which at best holds approximately in closed-loop. Both methods also model two resets per input period only, known to not hold generally [28]. Another frequency-domain method was suggested by [35], which computes the closed-loop directly by solving numerically. This yields a precise solution at the cost of being computationally intensive and not providing a link between open- and closed-loop. None of the available methods sufficiently links open-loop RC design, especially considering the underlying linear system to closed-loop behaviour. Without such a link RC design is impaired, as it is not clear how certain tuning choices affect the closed-loop performance. This work aims to bridge this gap.

Some authors have mentioned that RC can be modelled as a linear controller with a train of state-dependent weighted impulse inputs [22,36,37], but this idea is only developed for a CI [22] and for certain nonlinear systems [38], and not with the objective to find a frequency-domain solution. This work takes the impulsive RC modelling and generalizes that to obtain a closed-loop frequency domain description of RC systems, exploiting the resulting linear controller model, enabling accurate computation of closed-loop solutions in a way compatible to the industry preferred loop-shaping methodology. This accurately connects open-loop RC design to its closed-loop performance.

The remainder of this paper is structured as follows. First, preliminaries of RC, including reset elements, definitions and stability results are given in Section 2. Existing frequency domain analysis methods are presented and evaluated in Section 3. Section 4 introduces the novel impulse formulation for a general RC in open-loop, irrespective of reset law, followed by a closed-loop formulation. This generic modelling approach for closed-loop reset control systems is the first major contribution of this paper.

All remaining sections of this paper focus on solving this impulsive closed-loop formulation analytically in the frequency domain and demonstrating the accuracy and limitations of this solution. The first step to this goal is taken in Section 5 by rewriting the result into the frequency-domain which is essential for industry usage. Only systems with zero-crossing reset laws are considered from there on. This modelling is then simplified in Section 6 using clearly stated assumptions to allow for an analytical solution. This novel analytical approximation is the second contribution of this paper, providing insight in the closed-loop behaviour of reset control systems. Section 7 states the setup used to examine the obtained closed-loop description. The implications of the assumptions introduced in Section 6 are evaluated in Section 8. Afterwards, the accuracy and limitations of the obtained analytical approximation are evaluated in Section 9 by using controllers tuned for various specifications. Last, Section 10 concludes this paper.

2. Preliminaries on reset control

This section presents a generic reset control framework, along with relevant definitions and a stability theorem often used with reset control systems.

2.1. Reset control

Consider the generic closed-loop setup given in Fig. 1, consisting of linear systems K and G surrounding the reset element $\vec{R}$, with input $\vec{r}_l(t)$ and output $\vec{y}(t)$. Let $\vec{y}(t)$, $\vec{e}(t)$, $\vec{r}_l(t) \in \mathbb{R}^{m_y}$, $\vec{z}(t) \in \mathbb{R}^{m_z}$ and $\vec{q}(t) \in \mathbb{R}^{m_q}$, with m_y, m_z, $m_q \in \mathbb{N}$. Definition 1 defines $\vec{R}$, Definition 2 the reset types under consideration and Definition 3 the closed-loop as given in Fig. 1.

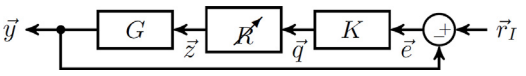

Fig. 1. Block diagram of a RCS with input $\vec{r}_I$ and output $\vec{y}$, consisting of reset element $\vec{R}$ surrounded by linear systems K and G.

These definitions permit MIMO implementations. Hence, Fig. 1 is drawn from right to left, as conventional to MIMO systems.

Definition 1.

Let a Reset Controller (RC) $\vec{R} : \vec{q}(t) \mapsto \vec{z}(t)$ be defined by dimension-compatible matrices A_R, B_R, C_R, D_R, states $\vec{x}(t) \in \mathbb{R}^{n_{ol}}$, $n_{ol} \in \mathbb{N}$ and reset matrices $A_{\rho,r}$. A reset occurs when $t = t_{r,ol} \in t_{R,ol}$, where $t_{R,ol}$ denotes the set of all reset time instants, and $t_{r,ol} \in t_{R,ol}$ representing any particular reset instant. Each $A_{\rho,r}$ corresponds to some subset of $t_{R,ol}$. The following equations describe $\vec{R}$:

$$\vec{R} : \begin{cases} \dot{\vec{x}}(t) = A_R\,\vec{x}(t) + B_R\,\vec{q}(t), & t \notin t_{R,ol} \\ \vec{x}^{+}(t) = A_{\rho,r}\,\vec{x}(t), & t \in t_{R,ol} \\ \vec{z}(t) = C_R\,\vec{x}(t) + D_R\,\vec{q}(t) \end{cases} \tag{1}$$

After-reset states are denoted by $\vec{x}^{+}$. Description (1) permits a MIMO RC and an arbitrary reset law.

Definition 2 (*Reset Types*)**.** In literature, the reset matrix A_ρ is generally diagonal and can also be non-constant. A fixed matrix is considered in this work and the subscript r is removed: $A_\rho = \text{diag}\left(\gamma_1, \ldots, \gamma_{n_{ol}}\right)$, with values $\gamma_i \in [-1, 1]$, $i \in \{1, \ldots, n_{ol}\}$. Define the following:

- Fully resetting RC: $\gamma_i \in \{0, 1\}$, $\forall\, i$ and $\exists\, i \mid \gamma_i = 0$.
- Partially resetting RC: A_ρ where $\exists\, i \mid \gamma_i \notin \{0, 1\}$.

Definition 3 (*Reset Control System (RCS)*)**.** Let the closed-loop reset control system $\vec{\mathcal{T}} : \vec{r}_I(t) \mapsto \vec{y}(t)$ as in Fig. 1 be defined by dimension-compatible matrices A_{cl}, B_{cl}, C_{cl}, D_{cl} and $A_{\rho cl}$, with states $\vec{x}_{cl} \in \mathbb{R}^{n_{cl}}$, $n_{cl} = (n_{ol} + n_K + n_G) \in \mathbb{N}$. A reset occurs when $t = t_r \in t_R$, where t_R denotes the set of all reset time instants and $t_r \in t_R$ any particular reset instant. $\vec{\mathcal{T}}$ is described by:

$$\vec{\mathcal{T}} : \begin{cases} \dot{\vec{x}}_{cl}(t) = A_{cl}\,\vec{x}_{cl}(t) + B_{cl}\,\vec{r}_I(t), & t \notin t_R \\ \vec{x}_{cl}^{+}(t) = A_{\rho cl}\,\vec{x}_{cl}(t), & t \in t_R \\ \vec{y}(t) = C_{cl}\,\vec{x}_{cl}(t) + D_{cl}\,\vec{r}_I(t) \end{cases} \tag{2}$$

RCs as in (1), (2) are SISO if $m_y = 1$, $m_z = 1$ and $m_y = 1$. Note that henceforth RC refers to the open-loop nonlinear controller and RCS refers to the closed-loop reset system.

Definition 4 (*Base-Linear System (BLS)*)**.** The base-linear system of Fig. 1 is obtained by removing all resets from the RCS, rendering it linear. Let R_L denote $\vec{R}$ without reset action:

$$R_L(s) \triangleq C_R\,(sI - A_R)^{-1}\,B_R + D_R \tag{3}$$

The BLS sensitivity function $S_L(s)$ and complementary sensitivity function $T_L(s)$ are given by:

$$S_L(s) \triangleq \ (I + G(s)\,R_L(s)\,K(s))^{-1} \tag{4}$$

$$T_L(s) \triangleq G(s)\,R_L(s)\,K(s)\ (I + G(s)\,R_L(s)\,K(s))^{-1} \tag{5}$$

Definition 5 (*Time Regularization*)**.** Time regularization removes any reset instance t_r from t_R if $t_r < t_p + \tau$, with $\tau > 0$ a tunable parameter and t_p the last occurred reset time instant in t_R [14]. Thus, if $\tau > 0$, all time instances $t_r \in t_R$ are distinct.

Definition 6 (*Zero-Crossing Law*)**.** A SISO RCS with zero-crossing law resets when $t_R = \left\{t \in \mathbb{R} \mid \vec{q}(t) = 0\right\}$.

RC systems can be prone to deadlock, beating and Zeno behaviour [28], causing solutions to be ill-defined. This behaviour can be avoided by using time regularization, by setting $\tau > 0$ [14,39]. Any practical discrete-time implementation inherently features time regularization, having τ equal to the sampling time [40]. In this work a practical setup is considered. Therefore, it is chosen to disregard deadlock, beating and Zenoness in this paper, as $\tau > 0$ automatically holds for often-used digitized implementations. As such, solutions to (2) are assumed to be well-defined.

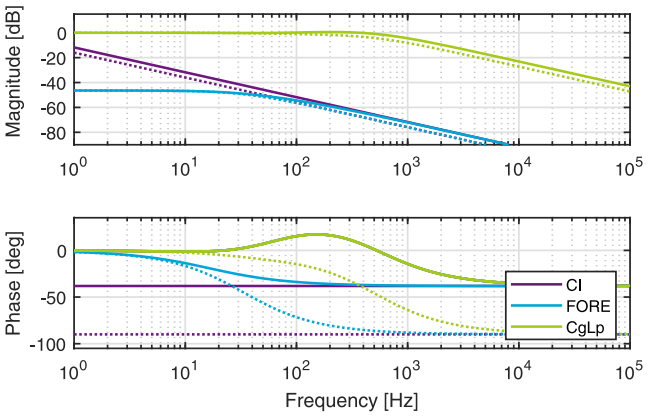

Fig. 2. Bode Plot with the linear, R_L (dashed line), and first harmonic, R_{DF} (solid line), responses for a CI, FORE and CgLp reset element. The harmonic responses, computed through DF analysis (10), use full reset ($\gamma = 0$).

2.2. Reset elements

Various reset elements are presented in literature. A few relevant ones are given below, all of them most commonly using zero-crossing reset laws. Fig. 2 gives the Bode plots for these, depicting their base-linear and nonlinear first harmonic responses.

2.2.1. Generalized Clegg Integrator (GCI)

The Clegg Integrator [3] is a resetting integrator, which can be generalized by allowing partial resets through γ. The GCI is defined with:

$$A_R = 0,\ B_R = 1\ C_R = 1,\ D_R = 0,\ A_\rho = \gamma \tag{6}$$

2.2.2. Generalized First Order Reset Element (GFORE)

FORE is based on a first order low-pass filter. It was first given by [5] and later generalized by permitting partial resets [17]. A GFORE with corner frequency ω_r is given with:

$$A_R = -\omega_r,\ B_R = \omega_r,\ C_R = 1,\ D_R = 0,\ A_\rho = \gamma \tag{7}$$

2.2.3. Constant in gain, Lead in phase (CgLp)

CgLp is a novel RC element providing broadband phase lead while maintaining unit gain [32]. This characteristic enables CgLp to be combined with any linear controller, increasing phase without inflicting gain alterations. This is achieved by merging a GFORE, having pole $\omega_{r\alpha}$, with a lead–lag filter, having pole ω_f and zero $\omega_r = \omega_{r\alpha}\,\alpha$. Parameter α corrects for the GFORE pole shift induced by reset nonlinearity [32], ensuring that the GFORE pole remains coincident with the lead–lag zero.

$$\left[\begin{array}{c|c} A_R & B_R \\ \hline C_R & D_R \end{array}\right] = \left[\begin{array}{cc|c} -\omega_{r\alpha} & 0 & \omega_{r\alpha} \\ \omega_f & -\omega_f & 0 \\ \hline \omega_f\,/\,\omega_r & 1-\omega_f\,/\,\omega_r & 0 \end{array}\right] \tag{8}$$

$$A_\rho = \mathrm{diag}\,[\gamma,\ 1]$$

2.3. Stability

Consider a SISO RCS where the matrices A_{cl}, C_{cl}, $A_{\rho cl}$ and A_ρ can be structured as below. This factorization is always possible if $G(s)$ has no direct feed-through.

$$A_{cl} = \begin{bmatrix} \bullet & \bullet \\ \bullet & A_R \end{bmatrix} \quad A_{\rho cl} = \begin{bmatrix} I_{n_{cl}-n_{ol}} & 0 \\ 0 & A_\rho \end{bmatrix}$$
$$C_{cl} = \begin{bmatrix} C_G & 0 \end{bmatrix} \quad A_\rho = \begin{bmatrix} I_{\tilde{\rho}} & 0 \\ 0 & A_\rho^* \end{bmatrix}$$

where $\bullet$ denotes any matrix. $A_\rho^* \in \mathbb{R}^{n_\rho \times n_\rho}$, $n_\rho \in \mathbb{N}_0$ is a matrix corresponding to the n_ρ resetting states. It follows that the number of non-reset states is $n_{\tilde{\rho}} = n_{ol} - n_\rho$.

Table 1
Overview of assumptions existing methods for computing frequency-domain closed-loop RC behaviour use. Empty fields indicate that there are no assumptions.

	DF	CL-DF	CL-FR
Modelled resets per period:	2	2	
Signals assumed sinusoidal:	$\vec{q}(t)$	$\vec{r}_l(t)$	$\vec{r}_l(t)$
Resets assumed at:		$\vec{q}_{DF,1} = 0$	
Neglects harmonics:	Yes		

Definition 7 ($\mathcal{H}_\beta$ - *Condition [9]*)**.**
A SISO RCS (2) with zero-crossing reset law, having all inputs $\vec{r}_l$ equal to 0, satisfies the $\mathcal{H}_\beta$ condition if $\exists\ \beta \in \mathbb{R}^{n_\rho}$, $P_\rho \in \mathbb{R}^{n_\rho \times n_\rho} > 0$, such that

$$\mathcal{H}_\beta \triangleq \begin{bmatrix} \beta\, C_G & 0_{n_\rho \times n_{\tilde{\rho}}} & P_\rho \end{bmatrix} (sI - A_{cl})^{-1} \begin{bmatrix} 0 \\ 0_{n_{\tilde{\rho}} \times n_\rho} \\ I_{n_\rho \times n_\rho} \end{bmatrix}$$

is strictly positive real, $A_{\rho cl}$ is non-zero and [41]:

$$A_\rho^{\star\,T} P_\rho A_\rho^\star - P_\rho \leq 0$$

Theorem 1 ($\mathcal{H}_\beta$ - *Stability [9,35]*)**.**
A SISO RCS (2) with a zero-crossing reset law is quadratically stable if and only if it satisfies $\mathcal{H}_\beta$ condition. Uniform exponential convergence and input-to-state convergence also hold if (2) satisfies $\mathcal{H}_\beta$.

3. Frequency-domain describing methods

The available frequency-domain methods for describing RCs are given in this section. These methods are applicable to zero-crossing resets only. Table 1 provides an overview of the various assumptions used by methods describing RCSs. The analytical approximation to RCSs developed in this paper will be juxtaposed against these existing methods in Section 9.

3.1. DF and HOSIDF analysis

Analysing SISO RCs in the frequency domain is typically performed using DF analysis, which computes the first harmonic in the Fourier series expansion of $\vec{z}(t)$. This requires (1) to have a globally asymptotically stable $2\,\pi\,/\,\omega$ - periodic output $\vec{z}(t)$, for a sinusoidal input $\vec{q}(t)$ with frequency $\omega > 0$. This happens if and only if [10]:

$$\left|\lambda\left(A_\rho\, e^{A_R\,\delta}\right)\right| < 1, \quad \forall\ \delta \in \mathbb{R}^+ \tag{9}$$

DF analysis is extended to Higher Order Sinusoidal Input Describing Function (HOSIDF) analysis by also considering the harmonics in the Fourier series expansion of $\vec{z}(t)$. [34].

Theorem 2 (*DF [10], HOSIDF [42]*)**.** *The nth order HOSIDF for an open-loop SISO RC (1) satisfying (9) with zero-crossing resets and a sinusoidal input with frequency $\omega > 0$ is computed by:*

$$R_{DF,n}(\omega) \triangleq C_R(j\omega n\, I - A_R)^{-1} \times \begin{cases} (I + j\theta_D(\omega))\ B_R + D_R, & n = 1 \\ j\theta_D(\omega)\, B_R, & \text{odd } n > 1 \\ 0, & \text{even } n > 1 \end{cases} \tag{10}$$

$$\begin{aligned} \text{where:}\quad \theta_D(\omega) &\triangleq -\frac{2\omega^2}{\pi}\, \Delta(\omega)\left[\Gamma_R(\omega) - \Lambda^{-1}(\omega)\right] \\ \Gamma_R(\omega) &\triangleq \Delta_R^{-1}(\omega) A_\rho\, \Delta(\omega)\, \Lambda^{-1}(\omega) \\ \Lambda(\omega) &\triangleq \omega^2 I + A_R^2 \\ \Delta(\omega) &\triangleq I + e^{\frac{\pi}{\omega} A_R} \\ \Delta_R(\omega) &\triangleq I + A_\rho\, e^{\frac{\pi}{\omega} A_R} \end{aligned}$$

DF analysis equals (10) taking only $n = 1$. The corresponding DF-approximated sensitivity function for (2) is:

$$S_{DF}(\omega) = \left(I + G(\omega)\, R_{DF,1}(\omega)\, K(\omega)\right)^{-1} \tag{11}$$

This approximation assumes (i) that all harmonics are negligible in closed-loop, (ii) $\vec{q}(t)$ to be sinusoidal, which (iii) implicitly assumes the RCS to have two resets per input period.

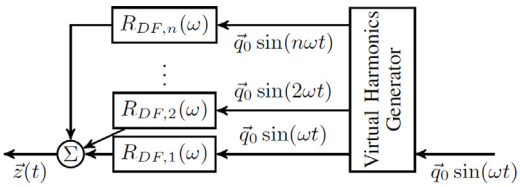

Fig. 3. HOSIDF representation of $\vec{R}$ for a sinusoidal input $\vec{q}(t)$, using a virtual harmonics generator.
Source: Adapted from [43].

HOSIDF analysis models the RC response in open-loop for input $\vec{q}(t) = \vec{q}_0 \sin(\omega t)$, as shown in Fig. 3 as:

$$Z(n\omega) = R_{DF,n}(\omega)\, Q(\omega) \tag{12}$$

$$\sum_{n=1}^{\infty} R_{DF,n}(\omega)\, Q(\omega) \Leftrightarrow \vec{R}(s)\, Q(s) \tag{13}$$

$$\vec{z}(t) = \sum_{n=1}^{\infty} \left| R_{DF,n}\, \vec{q}_0 \right| \sin(n\omega t + \angle R_{DF,n}) \tag{14}$$

The assumptions for S_{DF} do not hold. Reset induces harmonics, which through feedback prevent $\vec{q}(t)$ from being fully sinusoidal. RCSs often have more than two resets per period [28].

3.2. Closed-loop HOSIDF analysis

Recently a method was presented that extends HOSIDF to RCS [34]. Starting from open-loop HOSIDF, this method assumes (i) that there are exactly two resets per input period, spaced π / ω apart, and (ii) that solely the first harmonic, $Q(\omega) = K(\omega) S_{DF,1}(\omega)$, causes and affects resets.

Theorem 3 (*Closed-Loop HOSIDF (CL-DF) [34]*)**.** *The nth order CL-DF for an RCS with an input-to-state convergent SISO RC (1) satisfying (9), having zero-crossing resets and a sinusoidal input with frequency $\omega > 0$, is defined by:*

$$S_{DF_{CL},n}(\omega) \triangleq \begin{cases} Sl_1(\omega), & n = 1 \\ -Sl_{bls}(n\omega)\, L_n(\omega)\, Sl_{1,n}(\omega), & n > 1 \end{cases} \tag{15}$$

where:

$$\begin{aligned} L_n(\omega) &\triangleq G(n\omega)\, R_{DF,n}(\omega)\, K(\omega) \\ Sl_n(\omega) &\triangleq (I + L_n(\omega))^{-1} \\ L_{bls}(\omega) &\triangleq G(\omega)\, R_L(\omega)\, K(\omega) \\ Sl_{bls}(\omega) &\triangleq (I + L_{bls}(\omega))^{-1} \\ Sl_{1,n}(\omega) &\triangleq |Sl_1(\omega)|\, e^{jn\angle Sl_1(\omega)} \end{aligned}$$

CL-DF uses assumptions to close the loop, and hence introduces errors in modelling and prediction, yet improves upon S_{DF} as it includes harmonics. However, by considering all harmonics including the first together, it does not provide any link between the base-linear system and the RCS.

3.3. Closed-loop frequency response (CL-FR)

CL-FR is different from the other approaches mentioned, as it analyses a stable SISO RCS with zero-crossing resets and a sinusoidal input directly through numerical evaluation [35]. This direct closed-loop computation yields accurate results at the cost of not providing insight in how open-loop RC design translates to RCS performance.

4. Impulse reset modelling

Literature has shown that some RCs can be modelled as linear systems with a state-dependent timed impulse train input, a description first mentioned by [22]. Theorem 4 extends this result and proves that any general open-loop RC as in (1) can be equivalently modelled as a linear system with impulse inputs. This result is further developed in this section to acquire the RCS description, which is the first main result of this paper.

Theorem 4 (*Impulse-Based RC Modelling*). *The states $\dot{\vec{x}}(t)$ of any open-loop RC as in (1) are computed as:*

$$\dot{\vec{x}}(t) = A_R\,\vec{x}(t) + B_R\,\vec{q}(t) + \sum_{t_r \in t_R} (A_\rho - I)\,\vec{x}(t_r)\,\delta(t - t_r) \tag{16}$$

Proof. Consider an open-loop RC (1). The after-reset states $\vec{x}^+(t) \in \mathbb{R}^{n_{ol}}$ at $t = t_r \in t_R$ are given by:

$$\vec{x}^+(t) = A_\rho\,\vec{x}(t) = I\,\vec{x}(t) + (A_\rho - I)\,\vec{x}(t_r), \qquad t = t_r \in t_R$$

The term $(A_\rho - I)\vec{x}(t_r)$ is added at the reset instant, $t = t_r$. This can be modelled as a Heaviside step function, $H(t - t_r) \in \mathbb{R}^1$, weighted by $(A_\rho - I)\vec{x}(t_r)$. In [44], it is shown that, for functions $f(t)$ with piecewise discontinuities modelled by $H(t - t_r) \in \mathbb{R}^1$, the generalized derivative $\dot{f}(t)$ equals the classical derivative for all $t \neq t_r$, and a weighted Dirac delta function for all $t = t_r$. Per definition, $\dot{H}(t - t_r) = \delta(t - t_r)$, with $\delta(t)$ the Dirac delta function. Note that $\vec{x}(t_r)$ is sampled at $t = t_r$ and therefore is a constant, $\dot{\vec{x}}(t_r) = 0$. Inserting the Heaviside step function and differentiating gives:

$$\begin{aligned}
\vec{x}^+(t) &= \vec{x}(t) + (A_\rho - I)\,\vec{x}(t_r)\,H(t - t_r), && t = t_r \in t_R \\
\dot{\vec{x}}^+(t) &= \dot{\vec{x}}(t) + (A_\rho - I)\,\vec{x}(t_r)\,\delta(t - t_r), && t = t_r \in t_R \\
&= A_R\vec{x}(t) + B_R\,\vec{q}(t) + (A_\rho - I)\,\vec{x}(t_r)\,\delta(t - t_r), && t = t_r \in t_R
\end{aligned}$$

When $t \notin t_R$, no reset action occurs. The state flow is then governed by R_L (3):

$$\dot{\vec{x}}(t) = \begin{cases} A_R\vec{x}(t) + B_R\,\vec{q}(t) + (A_\rho - I)\,\vec{x}(t)\,\delta(t - t_r), & t = t_r \in t_R \\ A_R\vec{x}(t) + B_R\,\vec{q}(t), & t \notin t_R \end{cases}$$

This behaviour can be written in a more compact manner by summing $(A_\rho - I)\vec{x}(t)\delta(t - t_r)$ over all resets $t_r \in t_R$, completing this proof. □

Remark 4.1 (*Initial States*). Initial states are assumed to be zero throughout this section. It should be noted that reset times t_R often depend on the system state and thus on the initial conditions, e.g. in the case of zero-crossing reset laws, Definition 6. In Theorem 5 and Remark 5.1 the requirements for RCSs are stated by which this assumption is valid.

Corollary 4.1 (*RC Laplace Formulation*). *Let the transfer function $R_\delta(s)$ be defined by $R_\delta(s) \triangleq C_R\,(sI - A_R)^{-1}\,(A_\rho - I)$, the transfer between $Q(s)$ and $X(s)$ by $R_L^X(s) \triangleq (sI - A_R)^{-1}\,B_R$ and the reset response to $X(s)$ as $R_\delta^X(s) \triangleq (sI - A_R)^{-1}\,(A_\rho - I)$. The output and states of (1) are given in the Laplace domain by:*

$$Z(s) = R_L(s)\,Q(s) + R_\delta(s) \sum_{t_r \in t_R} \vec{x}(t_r)\,\mathrm{e}^{-t_r s} \tag{17}$$

$$X(s) = R_L^X(s)\,Q(s) + R_\delta^X(s) \sum_{t_r \in t_R} \vec{x}(t_r)\,\mathrm{e}^{-t_r s} \tag{18}$$

Proof. Start by writing (16) in the Laplace domain:

$$sX(s) = A_R\,X(s) + B_R\,Q(s) + \sum_{t_r \in t_R} \left(A_{\rho,k} - I\right)\,\vec{x}(t_r)\,\mathrm{e}^{-t_r s}$$

Vector $\vec{x}(t_r)$ is evaluated at a specific time instant and can therefore be treated as a constant. Rewriting for $X(s)$ and substitution of $R_L^X(s)$ and $R_{\delta,k}^X(s)$ gives (18). Solving for $X(s)$, using (1) to write $Z(s) = C_R\,X(s) + D_R\,Q(s)$ and afterwards inserting (18), $R_L(s)$ and $R_\delta(s)$ yields (17). □

The following corollaries state the first main contribution of this paper, by proving that any RCS can be described by the BLS summed with impulse responses.

Corollary 4.2 (*Closed-Loop $E(s)$*). *The RCS error response $E(s)$ is computed to be the BLS summed by impulse responses:*

$$E(s) = S_L(s)\,R_I(s) - S_L(s)\,G(s)R_\delta(s) \sum_{t_r \in t_R} \vec{x}(t_r)\,\mathrm{e}^{-t_r s} \tag{19}$$

The second term is denoted as $E_\delta(s, t_r)$ to simplify notation, giving

$$E(s) = S_L(s)\,R_I(s) + \sum_{t_r \in t_R} E_\delta(s, t_r)$$

Proof. From Fig. 1 it follows that $Q(s) = K(s)\,E(s)$. Together with (17) this gives:

$$Z(s) = R_L(s)\,K(s)\,E(s) + R_\delta(s) \sum_{t_r \in t_R} \vec{x}(t_r)\,\mathrm{e}^{-t_r s}$$

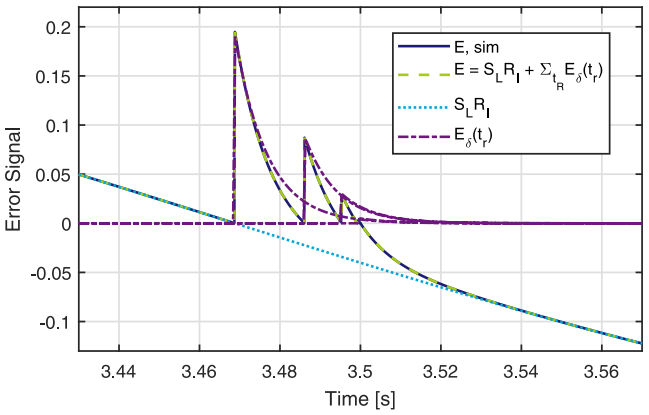

Fig. 4. Detail on a series of resets around a zero-crossing for a FORE closed-loop reset system as given by Example 4.1, using $\vec{r}_I = \sin(t / 2\pi)$. The components of (19), their sum and the simulated response are shown.

In Fig. 1 it is seen that $E(s) = R_I(s) - G(s)Z(s)$:

$$E(s) = R_I(s) - G(s)R_L(s)K(s)E(s) - G(s)R_\delta(s)\sum_{t_r \in t_R} \vec{x}(t_r)\,\mathrm{e}^{-t_r s}$$

The result follows by solving for $E(s)$ and inserting (4). □

Corollary 4.3 (*Closed-Loop $X(s)$*)**.** *The closed-loop states of $\vec{x}(s)$ are computed to be:*

$$\begin{aligned} X(s) &= R_L^X(s)K(s)S_L(s)R_I(s) \\ &\quad - R_L^X(s)K(s)S_L(s)G(s)R_\delta(s)\sum_{t_r \in t_R} \vec{x}(t_r)\,\mathrm{e}^{-t_r s} + R_\delta^X(s)\sum_{t_r \in t_R} \vec{x}(t_r)\,\mathrm{e}^{-t_r s} \end{aligned} \tag{20}$$

Proof. Take (18) and substitute $Q(s)$ with $K(s)E(s)$, using the RCS error $E(s)$ as defined by (19). □

Remark 4.2. All results based on Theorem 4 require uniqueness and existence of a solution to (1) only. No requirements on input types, system dimensions, stability or reset types are needed to compute the response. The RCS behaviour can thus be computed exactly, given that reset times t_R and corresponding states $\vec{x}(t_r)$ are known.

Remark 4.3. These results accept MIMO systems. However, MIMO reset control implementations often use multiple reset conditions [45,46]. The obtained results permit a straightforward extension to an arbitrary number of reset conditions, where each of these corresponds to some reset matrix $A_{\rho,r}$ and resets at some subset of reset times t_R. It follows that these results can describe closed-loop MIMO RC behaviour.

Example 4.1. Consider a SISO FORE in closed-loop with a zero-crossing reset law, using $K(s) = 100$, $G(s) = 1$, $\omega_r = 25$ and $\gamma = 0$. Fig. 4 illustrates in time-domain how the linear response $S_L(s)R_I(s)$ and impulse responses $E_\delta(s, t_r)$ are summed to create (19), which equals the simulated response.

Remark 4.4. Result (19) adds insight into RCS performance by linking how the base-linear system designed in open-loop and the introduction of reset in the form of impulses affects closed-loop performance. In closed-loop the RC behaves as the BLS, but having impulse responses with tunable weighting $I - A_\rho$ added to it. Thus, the closed-loop can be estimated by considering the BLS and weighted impulse response based on the open-loop design. This analysis allows to explain in a different way why RCs are found to have a lower sensitivity peak than their corresponding BLSs [11]. From (19) it follows that this must occur because impulse responses partially cancel out the BLS error.

5. Periodic results

Eq. (19) provides the first main contribution of this paper, by proving that any RCS equals a linear system summed by impulse responses. A precise RCS solution to this equation is obtained if the values t_R and $\vec{x}(t_r)$ as in (19) are computed. It might be possible to obtain these in a numerical manner to yield a precise and generic solution, without needing further assumptions or setup requirements. However, such a solution does not generally permit a frequency-domain

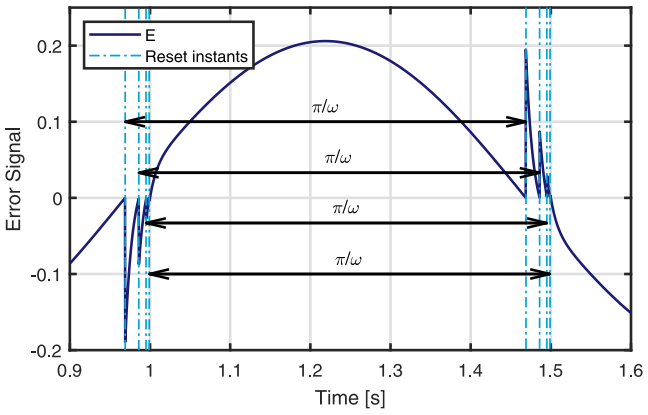

Fig. 5. Time response of a FORE RCS system satisfying Theorem 5 with indicated time intervals between resets, for $\vec{r}_l = \sin(t\ /\ 2\pi)$.

description, which is imperative for loop-shaping as desired by industry. The subsequent sections therefore aim to derive an analytical approximation to (19) in frequency-domain terms. This section first states conditions for RCS periodicity. Next, a modified HOSIDF framework is provided. This periodicity is then used alongside the modified HOSIDF to rewrite (19) in frequency-domain terms. Section 6 will further develop this result and acquire the analytical approximation in the frequency domain.

5.1. Periodicity of RCS

To write (19) in frequency-domain terms it is necessary that periodicity of (19) is established.

Theorem 5 (*Periodic RCS [35]*)**.** *If a SISO RCS (2) with zero-crossing law (a) satisfies $\mathcal{H}_\beta$, and (b) has a purely sinusoidal $\vec{r}_l(t)$ with frequency ω, then, in steady-state, the RCS has (i) a unique periodic solution $\vec{x}_{cl}(t)$, $\vec{y}(t)$ with period $2\pi\ /\ \omega$, (ii) all even harmonics equal to zero, and (iii) a periodic pattern of reset instants with period $\pi\ /\ \omega$.*

Remark 5.1. The steady state SISO RCS response requires that the initial state response has converged and is negligible. This is valid for any RCS satisfying Theorem 5, as uniform exponential stability holds as stated in Theorem 1. Effects caused by initial states will thus converge to zero. Therefore, all subsequent derivations contain solely the input responses of (2), ignoring initial state responses which Theorem 5 has proven to decay.

Remark 5.2 (*[35]*)**.** Theorem 5 also holds if, instead of (2) satisfying $\mathcal{H}_\beta$, it is Uniformly Bounded Steady-State.

Example 5.1. Fig. 5 gives the steady-state time response of the RCS given by Example 4.1 to a 1 Hz sinusoidal reference. This setup meets the requirements of Theorem 5, which therefore predicts that reset instants have a $\pi\ /\ \omega$ periodic pattern, and that the RCS has a unique periodic solution with period $2\pi\ /\ \omega$. Fig. 5 illustrates this by showing the $\pi\ /\ \omega$ time period between all pairs of equal-sized, sign-reversed reset impulses.

Corollary 5.1 utilizes the periodicity established by Theorem 5. A mathematical expression is obtained that will be needed to derive Theorem 7.

Corollary 5.1 (*Periodic Impulse Response*)**.** *Define a new set of reset times, $t = t_r \in t_\rho$ with $t_\rho = \{t \in t_R \mid t \in [0,\ \pi\ /\ \omega\rangle\}$. If Theorem 5 is satisfied the following simplification holds:*

$$R_\delta(s) \sum_{t_r \in t_R} \vec{x}(t_r)\, \mathrm{e}^{-t_r s} = \sum_{t_r \in t_\rho} \xi\left(s, t_r, \vec{x}(t_r)\right) \tag{21}$$

The term $\xi\left(s, t_r, \vec{x}(t_r)\right)$ is by definition $2\pi\ /\ \omega$ periodic:

$$\xi\left(s, t_r, \vec{x}(t_r)\right) \triangleq R_\delta(s) \sum_{p\,\in\, 2\mathbb{Z}} \left(\vec{x}(t_r)\, \mathrm{e}^{-(t_r + p\frac{\pi}{\omega})s} - \vec{x}(t_r)\, \mathrm{e}^{-(t_r + (p+1)\frac{\pi}{\omega})s}\right)$$

Proof. If Theorem 5 is satisfied, the reset instants are $\pi\ /\ \omega$ periodic. As such, t_ρ can be used to represent all resets, $\cup_p\{t_\rho + p\,\pi\ /\ \omega\} = t_R,\ \ p \in \mathbb{Z}$. These are thus equal:

$$\sum_{t_r \in t_R} \vec{x}(t_r)\, \mathrm{e}^{-t_r s} = \sum_{t_r \in t_\rho} \sum_{p \in \mathbb{Z}} \vec{x}(t_r + p\,\pi\ /\ \omega)\, \mathrm{e}^{-(t_r + p\frac{\pi}{\omega})s}$$

Using Theorem 5, $\vec{x}(t_r + p\,\pi\ /\ \omega)$ can be expressed in $\vec{x}(t_r)$.

$$\sum_{t_r \in t_R} \vec{x}(t_r)\, \mathrm{e}^{-\,t_r\, s} = \sum_{t_r \in t_\rho} \sum_{p\,\in\, 2\mathbb{Z}} \left(\vec{x}(t_r)\, \mathrm{e}^{-\,(t_r + p\frac{\pi}{\omega})s} \; - \vec{x}(t_r)\, \mathrm{e}^{-\,(t_r + (p+1)\frac{\pi}{\omega})s} \right)$$

Pre-multiplication with $R_\delta(s)$ and inserting $\xi\left(s, t_r, \vec{x}(t_r)\right)$ as defined above completes the proof. □

5.2. Impulse HOSIDF analysis

HOSIDF describes the RC response, as given by (16), thus modelling both the periodic impulse responses and the base-linear response to the input. As proven by Corollary 4.2, any closed-loop response equals the BLS summed by several impulse responses. Therefore, it is convenient to split the BLS and the various impulses in further derivations. To this end, Impulse HOSIDF is introduced in Definition 8. Impulse HOSIDF is identical to conventional HOSIDF in terms of higher harmonics. Solely the first harmonic is modified, by removing the base-linear response. As such, Impulse HOSIDF only captures the impulse responses. Definition 8 defines Impulse HOSIDF and provides its mathematical relation to the conventional HOSIDF [42].

Definition 8 (*Impulse HOSIDF*)**.** The nth order impulse HOSIDF analysis for a SISO RC (1) satisfying (9) with zero-crossing resets, given a sinusoidal input with frequency $\omega > 0$, is defined as a function of input matrix $B^\star$:

$$\begin{aligned} R^\star_{DF,n}(\omega, B^\star) &\triangleq C_R \left(j\omega\, n\, I - A_R\right)^{-1} \\ &\times \begin{cases} j\theta_D(\omega) B^\star, & \text{odd } n > 0 \\ 0, & \text{even } n > 1 \end{cases} \end{aligned} \tag{22}$$

If $B^\star = B_R$, HOSIDF and Impulse HOSIDF relate according to:

$$R_{DF,n}(\omega) = \begin{cases} R^\star_{DF,1}(\omega,\ B_R) + R_L(\omega), & n = 1 \\ R^\star_{DF,n>1}(\omega,\ B_R), & n > 1 \end{cases} \tag{23}$$

5.3. Closed-loop frequency-domain description

This section shows that open-loop Impulse HOSIDF can be used to exactly model RCSs (2) through the computation of a virtual input $Q^\star$ and input matrix $B^\star$. The open-loop states are first established for Impulse HOSIDF.

Lemma 5.1. *The following is used to simplify results:*

$$\mathrm{Re}\left\{(j\omega\, I - A_R)^{-1} j\right\} \equiv \left(\omega^2\, I + A_R^2\right)^{-1} \omega\, I \tag{24}$$

$$\mathrm{Re}\left\{(j\omega\, I - A_R)^{-1}\right\} \equiv -\left(\omega^2\, I^2 + A_R^2\right)^{-1} A_R \tag{25}$$

Theorem 6 (*Open-Loop States $\vec{x}(t_r)$*)**.** *Consider an open-loop SISO RC (1) using zero-crossing resets with a sinusoidal input $\vec{q}(t)$ having amplitude $\vec{q}_0 \in \mathbb{R}$ and frequency ω. Define reset sets based on the derivative $\dot{\vec{q}}(t)$:*

$$t_r^{\downarrow} \in t_R^{\downarrow} = \{t \in t_R : \dot{\vec{q}}(t) < 0\}$$
$$t_r^{\uparrow} \in t_R^{\uparrow} = \{t \in t_R : \dot{\vec{q}}(t) > 0\}$$

so that $t_R^{\downarrow} \cup t_R^{\uparrow} = t_R$. The states $\vec{x}(t_r^{\downarrow})$ obey:

$$\vec{x}(t_r^{\downarrow}) = \left(I + \mathrm{e}^{A_R \frac{\pi}{\omega}} A_\rho\right)^{-1} \left(I + \mathrm{e}^{A_R \frac{\pi}{\omega}}\right) \left(\omega^2\, I + A_R^2\right)^{-1} \omega\, I\, B_R\, \vec{q}_{\mathbf{0}} \tag{26}$$

where $(I + \mathrm{e}^{A_R \frac{\pi}{\omega}} A_\rho)$ is required to be invertible. This requirement is, for any RCS (1) with A_ρ diagonal as is conventional, always satisfied if the HOSIDF (10) exists, which needs $\Delta_R(\omega) = I + \left(A_\rho \mathrm{e}^{A_R \frac{\pi}{\omega}}\right)$ to be invertible.

Proof. Split the open-loop states (18) in two parts, so that $X(s) = X_L(s) + X_\delta(s)$:

$$X_L(s) = R_L^X(s)\, Q(s)$$
$$X_\delta(s) = R_\delta^X(s) \sum_{t_r \in t_R} \vec{x}(t_r)\, \mathrm{e}^{-\,t_r\, s}$$

First consider the linear term, $X_L(s)$. States $\vec{x}_L(t)$ can be obtained by taking the real part of $X_L(s) = X_L(j\omega)$ evaluated at some time instance. This is possible because of linearity combined with having a sinusoidal input. Rewriting the sinusoidal input $\vec{q}(t)$ gives:

$$\vec{q}(t) = \vec{q}_0\ \sin(\omega t) = \mathrm{Im}\{\vec{q}_0\, \mathrm{e}^{j\omega t}\} = \mathrm{Re}\{\vec{q}_0\, \mathrm{e}^{j(\omega t - \frac{\pi}{2})}\}$$

This is used to write $X_L(j\omega)$ in time domain:

$$X_L(j\omega) = (j\omega I - A_R)^{-1} B_R\, Q(j\omega)$$
$$\vec{x}_L(t) = \mathrm{Re}\{(j\omega I - A_R)^{-1} B_R\, \vec{q}_0\, e^{j(\omega t - \frac{\pi}{2})}\}$$

The zero-crossing reset law is used to determine $\vec{x}_L(t_r^{\downarrow})$, which requires finding $\vec{q}(t_r^{\downarrow})$. A zero-crossing of $\vec{q}(t)$ implies $\mathrm{Re}\{\vec{q}(t_r)\} = 0 \Leftrightarrow \vec{q}_0\, e^{j(\omega t - \frac{\pi}{2})} = \pm j\vec{q}_0$. As $\omega > 0$, function $\vec{q}_0\, e^{j(\omega t - \frac{\pi}{2})}$ propagates counter-clockwise, implying that solution $+j\vec{q}_0$ occurs when sinusoid $\vec{q}(t)$ crosses 0 from above ($\dot{\vec{q}}(t) < 0$). Applying this and using (24) to simplify gives:

$$\vec{x}_L(t_r^{\downarrow}) = \mathrm{Re}\left\{(j\omega\, I - A_R)^{-1} B_R\, j\, \vec{q}_0\right\}$$
$$\vec{x}_L(t_r^{\downarrow}) = \left(\omega^2\, I + A_R^2\right)^{-1}\, \omega\, I\, B_R\, \vec{q}_0$$

The impulsive part is considered next. Write in time domain:

$$\vec{x}_\delta(t) = \sum_{t_r \in t_{R_{\leq t}}} e^{A_R(t - t_r)}(A_\rho - I)\,\vec{x}(t_r)$$

From $\vec{q}(t)$ it follows that resets are spaced $\pi\,/\,\omega$ apart. Thus,
$\forall\, t_r^{\downarrow} \in t_R^{\downarrow},\ \exists\, \tilde{t}_r^{\uparrow} \in t_R^{\uparrow} \mid t_r^{\downarrow} - \tilde{t}_r^{\uparrow} = \pi\,/\,\omega$. Evaluating at $t_r^{\downarrow}$ and expressing in terms of the states at the previous reset, $\vec{x}_\delta(\tilde{t}_r^{\uparrow})$:

$$\vec{x}_\delta(t_r^{\downarrow}) = e^{A_R(t_r^{\downarrow} - \tilde{t}_r^{\uparrow})}(A_\rho - I)\,\vec{x}(\tilde{t}_r^{\uparrow}) + e^{A_R(t_r^{\downarrow} - \tilde{t}_r^{\uparrow})} \sum_{t_r \in t_{R_{<\tilde{t}_r^{\uparrow}}}} e^{A_R(\tilde{t}_r^{\uparrow} - t_r)}(A_\rho - I)\,\vec{x}(t_r)$$

The last term is per definition equal to $\vec{x}_\delta(\tilde{t}_r^{\uparrow})$. Therefore,

$$\vec{x}_\delta(t_r^{\downarrow}) = e^{A_R(t_r^{\downarrow} - \tilde{t}_r^{\uparrow})}(A_\rho - I)\,\vec{x}(\tilde{t}_r^{\uparrow}) + e^{A_R(t_r^{\downarrow} - \tilde{t}_r^{\uparrow})}\,\vec{x}_\delta(\tilde{t}_r^{\uparrow})$$
$$\vec{x}_\delta(t_r^{\downarrow}) = e^{A_R\frac{\pi}{\omega}}\left((A_\rho - I)\,\vec{x}(\tilde{t}_r^{\uparrow}) + \vec{x}_\delta(\tilde{t}_r^{\uparrow})\right)$$

If (9) is satisfied, as required for HOSIDF analysis, $\vec{x}(t) = -\vec{x}(t + \pi\,/\,\omega)$ [10]. Inserting $t_r^{\downarrow}$, $\tilde{t}_r^{\uparrow}$ gives $\vec{x}(t_r^{\downarrow}) = -\vec{x}(\tilde{t}_r^{\uparrow})$. Expanding $\vec{x}(t)$ shows that
$\vec{x}(t_r^{\downarrow}) = \vec{x}_L(t_r^{\downarrow}) + \vec{x}_\delta(t_r^{\downarrow}) = -\vec{x}_L(\tilde{t}_r^{\uparrow}) - \vec{x}_\delta(\tilde{t}_r^{\uparrow})$. From $\vec{x}_L(t_r)$ having $\pm j\vec{q}_0$ solutions on alternating reset times $\vec{x}_L(\tilde{t}_r^{\downarrow}) = -\vec{x}_L(t_r^{\uparrow})$ follows. Thus, $\vec{x}_\delta(t_r^{\downarrow}) = -\vec{x}_\delta(t_r^{\uparrow})$. Inserting this and writing for $\vec{x}(t_r^{\downarrow})$ gives:

$$\vec{x}_\delta(t_r^{\downarrow}) = e^{A_R\frac{\pi}{\omega}}\left((I - A_\rho)\,\vec{x}_L(t_r^{\downarrow}) - A_\rho\,\vec{x}_\delta(t_r^{\downarrow})\right)$$

Solving for $\vec{x}_\delta(t_r^{\downarrow})$ in terms of $\vec{x}_L(t_r^{\downarrow})$ and inserting that in $\vec{x}(t_r^{\downarrow}) = \vec{x}_L(t_r^{\downarrow}) + \vec{x}_\delta(t_r^{\downarrow})$ yields the desired solution. □

Remark 6.1. These states $\vec{x}_\delta(t_r^{\downarrow})$ equal those of the Impulse HOSIDF case, given that $B_R = B^\star$ and $Q(\omega) = Q^\star(\omega)$.

Next, the virtual input $Q^\star(\omega)$ to the Impulse HOSIDF and corresponding input matrix $B^\star$ are computed as a function of $\vec{x}(t_r^{\downarrow})$. These are then used to find the closed-loop formulation.

Corollary 6.1 (*Impulse HOSIDF Can Model Any $\vec{x}(t_r^{\downarrow})$*)**.** *Impulse HOSIDF (22) can model any periodic impulse response with states $\vec{x}(t_r^{\downarrow})$ by choosing the virtual input magnitude $\vec{q}_0^\star(\omega, \vec{x}(t_r^{\downarrow})) = 1$ and the input matrix $B^\star(\omega, \vec{x}(t_r^{\downarrow}))$ as:*

$$B^\star(\omega, \vec{x}(t_r^{\downarrow})) = \zeta(\omega)\,\vec{x}(t_r^{\downarrow}) \tag{27}$$

with $\zeta(\omega)$ defined as:

$$\zeta(\omega) = \omega^{-1}\left(\omega^2\, I + A_R^2\right)\left(I + e^{A_R\frac{\pi}{\omega}}\right)^{-1}\left(I + e^{A_R\frac{\pi}{\omega}} A_\rho\right)$$

Proof. Substitution of $B^\star(\omega, \vec{x}(t_r^{\downarrow}))$ for B_R in (26) while using virtual input $Q^\star(\omega, \vec{x}(t_r^{\downarrow}))$ with magnitude $\vec{q}_0^\star(\omega, \vec{x}(t_r^{\downarrow})) = 1$ instead of $Q(\omega)$, and rewriting for $B^\star(\omega, \vec{x}(t_r^{\downarrow}))$ afterwards, yields the result. This shows that by computing $B^\star(\omega, \vec{x}(t_r^{\downarrow}))$ any periodic reset state can be created, and hence that Impulse HOSIDF can model any periodic impulse response.
$B^\star(\omega, \vec{x}(t_r^{\downarrow}))$ makes magnitude $\vec{q}_0^\star(\omega, \vec{x}(t_r^{\downarrow}))$ obsolete, which is why
$q_0^\star(\omega, \vec{x}(t_r^{\downarrow})) = 1$ is chosen. The phase of $Q^\star(\omega)$ determines reset times, which is covered in a later section. □

Theorem 7 (*Impulse HOSIDF Analysis in Closed-Loop*)**.** *A summation of Impulse HOSIDF responses on top of the BLS can accurately describe $e(t)$ for any system satisfying Theorem 5, given continuity of $\vec{e}(t)$ ($\vec{e}(t) \in C^0$):*

$$E(\omega) = S_L(\omega)\,R_I(\omega) - S_L(\omega)\,G(\omega) \sum_{t_\rho} R^\star_{DF,1}(\omega, B^\star(\omega, \vec{x}(t_r^{\downarrow})))\,Q^\star(\omega, \vec{x}(t_r^{\downarrow})) \tag{28}$$

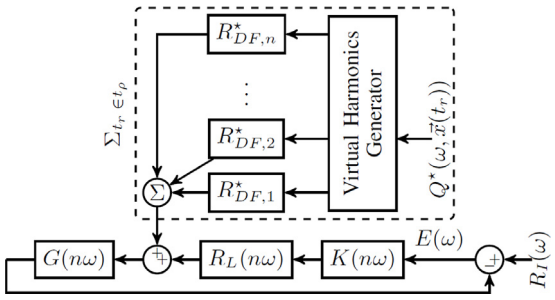

Fig. 6. Block diagram representing (28). The dashed area must be summed over all $t_r \in t_\rho$. Arguments of $R^\star_{DF,n}(\omega, B^\star(\omega, \vec{x}(t_r^\downarrow)))$ are dropped.

$$E(n\omega) = -S_L(n\omega)\, G(n\omega) \sum_{t_\rho} R^\star_{DF,n}(\omega, B^\star(\omega, \vec{x}(t_r^\downarrow)))\, Q^\star(\omega, \vec{x}(t_r^\downarrow)) \tag{29}$$

with $Q^\star(\omega, \vec{x}(t_r^\downarrow))$ *having magnitude* 1 *and phase to ensure the correct reset times. Fig. 6 represents* (28) and (29) *graphically.*

Proof. Take (12) and insert (23), with a designable input matrix $B_R = B^\star(\omega, \vec{x}(t_r^\downarrow))$ and sinusoidal input $Q^\star(\omega, \vec{x}(t_r^\downarrow))$ with amplitude 1. Arguments of $B^\star$ and $Q^\star$ are dropped.

$$Z(\omega) = R_L(\omega)\, Q^\star + R^\star_{DF,1}(\omega, B^\star)\, Q^\star$$
$$Z(n\omega) = R^\star_{DF,n}(\omega, B^\star)\, Q^\star$$

Inserting the open-loop $Z(\omega)$ (17), using $B^\star$ and $Q^\star$ computed according to the actual states $\vec{x}(t_r^\downarrow)$, and rewriting gives:

$$\sum_{n=1}^{\infty} R^\star_{DF,n}(\omega, B^\star)\, Q^\star = R_\delta(\omega) \sum_{t_r \in t_R} \vec{x}(t_r)\, \mathrm{e}^{-t_r j\omega}$$

The reset times $t = t_r \in t_R = \cup_p \{t_r + p\,\pi\ /\ \omega\},\ p = \mathbb{Z}$ follow from zero-input resets. Using these yields:

$$\sum_{n=1}^{\infty} R^\star_{DF,n}(\omega, B^\star)\, Q^\star = R_\delta(\omega) \sum_{p\,\in\,\mathbb{Z}} \vec{x}(t_r + p\,\pi\ /\ \omega)\ \mathrm{e}^{-(t_r + p\,\pi\ /\ \omega) j\omega}$$

The correct HOSIDF response for resets at t_ρ with weight $\vec{x}(t_r)$ is ensured if $B^\star$ and $Q^\star$ are computed according to Corollary 6.1. HOSIDF has odd harmonics only, thus $\vec{x}(t_r) = -\vec{x}(t_r + \pi\ /\ \omega)$. Simplifying using periodicity and inserting the definition of $\xi\left(s, t_r, \vec{x}(t_r)\right)$ from Corollary 5.1 gives:

$$\sum_{n=1}^{\infty} R^\star_{DF,n}(\omega, B^\star)\, Q^\star = R_\delta(\omega) \sum\nolimits_{p\,\in\,2\mathbb{Z}} \left(\vec{x}(t_r)\, \mathrm{e}^{-(t_r + p\frac{\pi}{\omega}) j\omega} - \vec{x}(t_r)\, \mathrm{e}^{-(t_r + (p+1)\frac{\pi}{\omega}) j\omega}\right)$$
$$\sum_{n=1}^{\infty} R^\star_{DF,n}(\omega, B^\star)\, Q^\star = \xi\left(\omega, t_r, \vec{x}(t_r)\right)$$

Thus far, this holds for open-loop Impulse HOSIDF. Conveniently, $\xi\left(s, t_r, \vec{x}(t_r)\right)$ as in (21) is obtained, which can be substituted in the closed-loop response (19), which requires inserting the closed-loop values for t_r and $\vec{x}(t_r)$. □

Remark 7.1. Theorem 7 proves that any SISO RC (2) with (i) zero-crossing resets (ii) satisfying the $\mathcal{H}_\beta$ condition and (iii) having $\vec{e}(t) \in C^0$ can be described without error by a summation of Impulse HOSIDF responses, if the set t_ρ and states $\vec{x}(t_r)$ are known $\forall\, t_r \in t_\rho$.

Remark 7.2. Theorem 7 also holds if $\vec{e}(t) \notin C^0$, except for prediction errors caused by the Gibbs phenomenon in the vicinity of discontinuities.

With (28) an accurate description is provided that can model the same RCSs in frequency-domain as CL-FR can, given that t_ρ and $\vec{x}(t_r)$ are known, without needing further conditions.

6. Analytical solution

To solve (28), time instants t_r and states $\vec{x}(t_r)$ must be computed $\forall\, t_r \in t_\rho$. This can be done numerically or analytically. For the sake of simplifying analysis and staying close to what is familiar to the linear control loop-shaping based

methodology, it is chosen to pursue an analytical solution. This choice comes at the cost of requiring assumptions, impacting precision. The effects of these assumptions are evaluated in Section 8. This section will introduce these assumptions and utilize these to obtain an analytical solution to (28), and thus approximate (19) analytically in the frequency domain for steady-state solutions.

Assumption 1 (*Two Resets Per Period*)**.** Assume that sufficient accuracy is achieved by modelling a RCS (2) satisfying Theorem 7 with exactly two resets per period, taking $t_\rho \in \mathbb{R}$. Accurate modelling of the two modelled resets requires that any unmodelled reset does not significantly influence their position nor states. This holds if the impulse responses are sufficiently convergent relative to the frequency of the reference sinusoid.

Assumption 2 (*Zero-Crossing Direction*)**.** It is assumed that at any reset the direction of $\vec{q}(t)$ crossing zero is equal to that predicted by the nearby BLS zero-crossing: $\operatorname{sign}(\dot{\vec{q}}(t)) = \operatorname{sign}(\dot{\vec{q}}_L(t)),\ \forall\, t \mid \vec{q}(t) = 0$. This holds for most RCSs given that they are sufficiently convergent, such that $\dot{\vec{q}}(t) \approx \dot{\vec{q}}_L(t),\ \forall\, t \in t_R$.

Assumption 3 (*Existence Of a Reset Instant*)**.** Assume that, at any reset instant, the absolute combined magnitude of all prior resets-induced impulse responses is less than the absolute peak value of the BLS response. This must hold in any real system satisfying Theorem 5. Otherwise, there cannot be a reset at $\pi\ /\ \omega$ distance from the previous reset, which contradicts Theorem 5. However, this assumption may be violated in cases where other assumptions affect solutions.

Lemma 7.1 (*Convergence*)**.** *The series $\sum_{p\,\in\,\mathbb{N}} \mathrm{e}^{Ap}$, where A is square, is convergent if all $\lambda\,(A) < 0$.*

Proof. Start by rewriting the problem into a Neumann series:

$$\sum_{p\,\in\,\mathbb{N}} \mathrm{e}^{A\,p} = \sum_{p\,\in\,\mathbb{N}} \left(\mathrm{e}^{A}\right)^{p}$$

This series converges if the spectral radius satisfies $\rho\,(\mathrm{e}^{A}) < 1$, thus if the eigenvalues $\lambda^\star$ corresponding to e^{A} satisfy $\max|\lambda^\star| < 1$. Because $\lambda^\star = \mathrm{e}^{\lambda}$, where λ denotes the eigenvalues of A, series convergence follows if $\nexists\ \lambda(A) \geq 0$. □

Lemma 7.2 (*Closed-Loop Reset Instant*)**.** *A RCS reset instant at a descending zero-crossing, $t_\rho^{\downarrow}$, can, for any RC satisfying Theorem 7, be computed using Assumptions 1 to 3:*

$$\omega\, t_\rho^{\downarrow} + \angle\,(K(j\omega)\,S_L(j\omega)\,R_I(j\omega)) + \Phi(\omega, \vec{x}(t_r^{\downarrow})) = \pi \tag{30}$$

This $t_\rho^{\downarrow}$ corresponds to the zero crossings of $Q^\star$ with:

$$\angle\, Q^\star(\omega) = \angle\,(K(j\omega)\,S_L(j\omega)\,R_I(j\omega)) + \Phi(\omega, \vec{x}(t_r^{\downarrow})) \tag{31}$$

If $\Phi(\omega, \vec{x}(t_r^{\downarrow})) = 0$, (30) computes the descending zero crossings of the BLS. Phase shift $\Phi(\omega, \vec{x}(t_r^{\downarrow}))$ is defined as:

$$\Phi(\omega, \vec{x}(t_r^{\downarrow})) \triangleq \sin^{-1}\left(C_Q \sum_{p\,\in\,2\mathbb{N}} \left(\mathrm{e}^{A_Q \frac{p\pi}{\omega}} - \mathrm{e}^{A_Q \frac{(p-1)\pi}{\omega}} \right) \right.$$
$$\left. \times\, B_Q\, \vec{x}(t_\rho)\ (|K(j\omega)\,S_L(j\omega)\,R_I(j\omega)|)^{-1} \right) \tag{32}$$

where A_Q, B_Q, C_Q and D_Q denoting state-space matrices of
$Q_\delta(s) = K(s)\,S_L(s)\,G(s)\,R_\delta(s)$. Lemma 7.1 states series convergence, which requires asymptotic stability of Q_δ. Set $\mathbb{N}$ is taken to exclude zero throughout this work.

Proof. Take (19) for a SISO RC and pre-multiply by $K(s)$ to acquire the closed-loop description of $Q(s)$:

$$Q(s) = K(s)\,S_L(s)\,R_I(s) - K(s)S_L(s)\,G(s)\,R_\delta(s) \sum_{t_r\,\in\,t_R} \vec{x}(t_r)\,\mathrm{e}^{-\,t_r\,s}$$

Combining Assumption 1 with Theorem 5 shows that $t_R = t_\rho + p\,\pi\ /\ \omega,\ \ p \in \mathbb{Z}$, where t_ρ has one entry. Inserting this and substituting $Q_\delta(s)$ as defined above gives:

$$Q(s) = K(s)\,S_L(s)\,R_I(s) - Q_\delta(s) \sum_{p\,\in\,\mathbb{Z}} \vec{x}(t_\rho + \frac{p\,\pi}{\omega})\,\mathrm{e}^{-\,(t_\rho + \frac{p\,\pi}{\omega})\,s}$$

Reset instant periodicity causes all resets instants prior to t_r to be at times $t_r - \frac{p\,\pi}{\omega},\ p \in \mathbb{N}$. The time-domain solution for $\vec{q}(t)$ is obtained for a sinusoidal r_l with frequency ω:

$$\begin{aligned}\vec{q}(t_r) = &\ |K(j\omega)\,S_L(j\omega)\,R_l(j\omega)| \ \times\ \sin\left(\omega t + \angle\left(K(j\omega)\,S_L(j\omega)\,R_l(j\omega)\right)\right)\\ &- \sum_{p\,\in\,\mathbb{N}} \left(C_Q\, \mathrm{e}^{A_Q \frac{p\pi}{\omega}}\, B_Q + D_Q\right) \vec{x}(t_\rho + \frac{p\,\pi}{\omega})\end{aligned}$$

where the impulse response is expressed in state-space terms. Corollary 4.1 shows that $R_\delta(s)$ has no direct feed-through, which by definition of $Q_\delta(s)$ implies that $D_Q = 0$.

The following expression is obtained by utilizing the periodicity of $\vec{x}(t)$ proven by Theorem 5:

$$\begin{aligned}\vec{q}(t_r) = &\ |K(j\omega)\,S_L(j\omega)\,R_l(j\omega)| \ \times\ \sin\left(\omega t_r + \angle\left(K(j\omega)\,S_L(j\omega)\,R_l(j\omega)\right)\right)\\ &+ C_Q \left(\sum_{p\,\in\,2\mathbb{N}} \mathrm{e}^{A_Q \frac{p\pi}{\omega}} - \mathrm{e}^{A_Q \frac{(p-1)\pi}{\omega}}\right) B_Q\, \vec{x}(t_r)\end{aligned}$$

Per definition of a zero-crossing reset law $\vec{q}(t_r) = 0$. Inserting this and taking the inverse sine gives, for $m \in \mathbb{Z}$:

$$\begin{aligned}m\,\pi \quad = &\ \omega\, t_r + \angle\left(K(j\omega)\,S_L(j\omega)\,R_l(j\omega)\right)\\ &+\ \sin^{-1}\Big[C_Q\ \textstyle\sum_{p\,\in\,2\mathbb{N}} \left(\mathrm{e}^{A_Q \frac{p\pi}{\omega}} - \mathrm{e}^{A_Q \frac{(p-1)\pi}{\omega}}\right)\\ &\times B_Q\, \vec{x}(t_r)\ \left(|K(j\omega)\,S_L(j\omega)\,R_l(j\omega)|\right)^{-1}\Big]\end{aligned}$$

The inverse sine exists if Assumption 3 holds. A descending zero-crossing occurs if the sinusoid argument is $m\,\pi$, with odd m. These cases correspond to $t = t_r^{\downarrow}$. The zero-crossing direction is assumed to be unaffected by prior resets by Assumption 2. The solution $m = 1$ is chosen. Inserting that while substituting $\Phi(\omega, \vec{x}(t_r^{\downarrow}))$ yields (30). Zero-crossings of a sinusoidal $Q^\star$ with phase (31) gives resets $t_\rho^{\downarrow} + p\,\pi\ /\ \omega$. □

Assumption 4 (*Small Effect of Resets on Reset Times*)**.** Assume that $\Phi(\omega, \vec{x}(t_\rho))$ (32) satisfies $\Phi(\omega, \vec{x}(t_\rho)) \ll \pi,\ \forall\ \omega$. This holds if reset times are close to the BLS zero crossings of $\vec{q}(t)$.

Lemma 7.3 (*States $\vec{x}(t_\rho^{\downarrow})$*)**.** *States $\vec{x}(t_\rho^{\downarrow})$ are, given Assumptions 1 to 4, for a system satisfying Theorem 5, computed by:*

$$\begin{aligned}\vec{x}(t_\rho^{\downarrow}) = &\left[I + \left(\omega^2\, I^2 + A_R^2\right)^{-1} A_R\, B_R\, C_Q \sum_{k\,\in\,2\mathbb{N}} \left(\mathrm{e}^{A_Q \frac{k\pi}{\omega}} - \mathrm{e}^{A_Q \frac{(k-1)\pi}{\omega}}\right) B_Q\right.\\ &\left. - 0.5\, C_H \sum_{k\,\in\,2\mathbb{N}} \left(\mathrm{e}^{A_H \frac{k\pi}{\omega}} - \mathrm{e}^{A_H \frac{(k-1)\pi}{\omega}}\right) B_H\right]^{-1}\\ &\times \left(\omega^2\, I + A_R^2\right)^{-1} \omega\, B_R\ |K(j\omega)\,S_L(j\omega)\,R_l(j\omega)|\end{aligned} \tag{33}$$

Which requires the inverted terms to be invertible. State-space matrices A_H, B_H, C_H and D_H correspond to $H(s)$:

$$H(s) = R_\delta^X(s) - R_L^X(s)\,K(s)\,S_L(s)\,G(s)\,R_\delta(s)$$

The two series converge if A_Q and A_H satisfy Lemma 7.1, thus if Q and H are asymptotically stable.

Proof. Consider (20) for a SISO RC and separate it into $X_L(s)$ and $X_\delta(s)$ such that $X(s) = X_L(s) + X_\delta(s)$:

$$\begin{aligned}X_L(s) &= R_L^X(s)\,K(s)\,S_L(s)\,R_l(s)\\ X_\delta(s) &= \left(R_\delta^X(s) - R_L^X(s)\,K(s)\,S_L(s)\,G(s)\,R_\delta(s)\right)\\ &\quad\times \sum_{t_r\,\in\,t_R} \vec{x}(t_r\ \in\ t_r)\,\mathrm{e}^{-\,t_r,\,s}\end{aligned}$$

Writing the linear term $\vec{x}_L(t)$ in time domain for a sinusoidal input, while using that $\vec{x}_L(t)$ is real, gives the following:

$$\vec{x}_L(t) = \mathrm{Re}\left\{R_L^X(j\omega)\ |K(j\omega)\,S_L(j\omega)\,R_l(j\omega)|\ \ \mathrm{e}^{j\omega(t-\frac{\pi}{2}) + j\angle\left(K(j\omega)\,S_L(j\omega)\,R_l(j\omega)\right)}\right\}$$

Evaluating at $t_\rho^{\downarrow}$ by rewriting and inserting (30) shows:

$$\vec{x}_L(t_\rho^{\downarrow}) = \mathrm{Re}\left\{R_L^X(j\omega)\ |K(j\omega)\,S_L(j\omega)\,R_l(j\omega)|\ \ \mathrm{e}^{j\left(\frac{\pi}{2}\ -\ \Phi(\omega, \vec{x}(t_{\rho\downarrow}))\right)}\right\}$$

Take $\Phi(\omega, \vec{x}(t_\rho^{\downarrow}))$ from (32) and apply Assumption 4, such that $\Phi(\omega, \vec{x}(t_\rho^{\downarrow})) = \sin^{-1}(\bullet) \approx (\bullet)$, where $\bullet$ denotes the terms within Φ. Then, the last term of $\vec{x}_L(t_\rho^{\downarrow})$ becomes $\mathrm{e}^{j(\frac{\pi}{2} - \bullet)}$. Given Assumption 4, the first Taylor expansion can be used,

giving the simplification $e^{j(\frac{\pi}{2}-\bullet)} \approx j + (\bullet)$. Inserting this and expanding $\Phi(\omega, \vec{x}(t_\rho^\downarrow))$ gives:

$$\vec{x}_L(t_\rho^\downarrow) = \mathrm{Re}\left\{ R_L^X(j\omega)\ |K(j\omega)S_L(j\omega)R_I(j\omega)| \times \left[j + C_Q \sum_{p\in 2\mathbb{N}} \left(e^{A_Q \frac{p\pi}{\omega}} - e^{A_Q \frac{(p-1)\pi}{\omega}} \right) \times B_Q\, \vec{x}(t_\rho^\downarrow)\ (|K(j\omega)S_L(j\omega)R_I(j\omega)|)^{-1} \right] \right\}$$

For a SISO RC this can be simplified to:

$$\vec{x}_L(t_\rho^\downarrow) = \mathrm{Re}\left\{ R_L^X(j\omega)\ |K(j\omega)S_L(j\omega)R_I(j\omega)|\ j + R_L^X(j\omega)C_Q \sum_{p\in 2\mathbb{N}} \left(e^{A_Q \frac{p\pi}{\omega}} - e^{A_Q \frac{(p-1)\pi}{\omega}} \right) B_Q\, \vec{x}(t_\rho^\downarrow) \right\}$$

Consider $X_\delta(s)$. Insert $H(s)$ and write in time domain. As $R_\delta(s)$ has no direct feed-through D_H must equal zero.

$$\vec{x}_\delta(t) = \sum_{t_r \in t_{R_{\leq t}}} \left(C_H\, e^{A_H(t-t_r)} B_H \right) \vec{x}(t_r)$$

Considering Assumption 1 with Theorem 5, such that all resets are spaced $\pi\ /\ \omega$ apart, and evaluating at $t_\rho^\downarrow$ gives:

$$\vec{x}_\delta(t_\rho^\downarrow) = C_H \sum_{p\in 2\mathbb{N}} \left(e^{A_H(\frac{p\pi}{\omega})} - e^{A_H(\frac{(p-1)\pi}{\omega})} \right) B_H\, \vec{x}(t_\rho^\downarrow)$$

Inserting these results into $\vec{x}(t_\rho^\downarrow) = \vec{x}_L(t_\rho^\downarrow) + \vec{x}_\delta(t_\rho^\downarrow)$, solving for $\vec{x}(t_\rho^\downarrow)$ and inserting (24), (25) gives the stated result. □

Theorem 8 states the main contribution of this paper, providing an analytical approximation for steady-state RCS behaviour in frequency-domain terms. This is an alternative to the description methods stated in Section 3. The corollaries stated afterwards provide several sensitivity functions.

Theorem 8 (*Analytical Solution for $E(\omega)$ (δ-CL)*)**.** *The error response of a RCS (2) satisfying Theorem 5, given Assumptions 1 to 4, is stated below. Arguments of $B^\star(\omega, \vec{x}(t_r^\downarrow))$ are dropped.*

$$E_{\delta-CL,n}(\omega) = S_L(\omega n) \times \begin{cases} R_I(\omega) - G(\omega) R^\star_{DF,1}(\omega, B^\star)\, \Psi(\omega, 1), & n = 1 \\ -G(\omega n) R^\star_{DF,n}(\omega, B^\star)\, \Psi(\omega, n), & n > 1 \end{cases} \tag{34}$$

where: (35)

$$\Psi(\omega, n) = \left(|K(\omega)S_L(\omega)R_I(\omega)| \times e^{nj\angle K(\omega)S_L(\omega)R_I(\omega) + nj\Phi(\omega, \vec{x}(t_r^\downarrow))} \right)$$

Definition 8 defines $R^\star_{DF,n}$. Parameters $\vec{x}(t_r^\downarrow)$, $\Phi(\omega, \vec{x}(t_r^\downarrow))$ and $B^\star(\omega, \vec{x}(t_r^\downarrow))$ are given by (33), (27) and (32), respectively.

Proof. Insert (33) into (27) to solve (28). Virtual input $Q^\star$ has magnitude 1, see Corollary 6.1, and phase (31). From Assumption 1 it follows that a summation over t_ρ is obsolete, as this set has one entry only. Rewriting gives the result.

These equations combine harmonic and reference frequencies. Multiplying the phase by n accounts for this. □

Corollary 8.1 (*Analytical solution for $S(\omega)$*)**.** *Sensitivity is defined as $S(\omega) = E(\omega)R_I(\omega)^{-1}$. Applying this to (34) while correcting the phase for harmonics gives:*

$$S_{\delta-CL,n}(\omega) = E_{\delta-CL,n}(\omega) \left(|R_I(\omega)|\, e^{nj\angle R_I(\omega)} \right)^{-1} \tag{36}$$

Corollary 8.2 (*Complementary Sensitivity*)**.** *The complementary sensitivity $T(\omega)$ is defined as $I - S(\omega)$:*

$$T_{\delta-CL,n}(\omega) = I - E_{\delta-CL,n}(\omega) \left(|R_I(\omega)|\, e^{nj\angle R_I(\omega)} \right) \tag{37}$$

Corollary 8.3 (*Control Sensitivity*)**.** *Split the linear system $G(s)$ in plant $P(s)$ and controller $C(s)$, $G(s) = P(S)C(S)$. Control input $U(s)$ enters $P(s)$: $Y(s) = P(s)U(s)$. The control input $CS(\omega) : \vec{r}_I(t) \mapsto \vec{u}(t) \triangleq CS(\omega) = P^{-1}(\omega)T(\omega)$:*

$$CS_{\delta-CL,n}(\omega) = P^{-1}(jn\omega)\, T_{\delta-CL,n}(\omega) \tag{38}$$

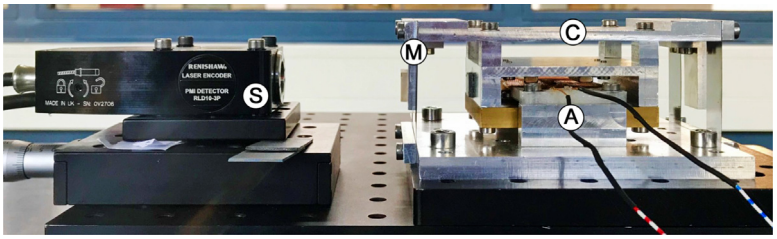

Fig. 7. 1 Degree-of-Freedom precision positioning stage that moves cart (C) using Lorentz actuator (A). This cart is attached to the frame by means of two leaf flexures, which constrain all movements but one translation. This translation is measured using laser encoder (S), which measures its distance relative to cart-fixed mirror (M).

The presented results can be transformed into time-domain signals using the following equations:

$$\vec{y}(t) \approx \sum_{n=1}^{\infty} \left|T_{DF,n}(\omega)\right| \sin(n\omega t + \angle T_{DF,n}(\omega)) \tag{39}$$

$$\vec{e}(t) \approx \sum_{n=1}^{\infty} \left|E_{DF,n}(\omega)\right| \sin(n\omega t + \angle E_{DF,n}(\omega)) \tag{40}$$

$$\vec{u}(t) \approx \sum_{n=1}^{\infty} \left|CS_{DF,n}(\omega)\right| \sin(n\omega t + \angle CS_{DF,n}(\omega)) \tag{41}$$

Thus far, frequency-domain descriptions are provided for pure sinusoidal inputs only. The following assumption extends the results by stating a condition that permits approximating RCSs with multi-sine inputs and disturbances.

Assumption 5 (*Superposition for Multi-Sine Inputs*)**.** Consider a closed-loop RC (2) with multiple sinusoidal references superimposed, having magnitudes R_{l_1} to $R_{l_{\bar{k}}}$, $\bar{k} \in \mathbb{N}$. Define the corresponding BLS magnitudes for $\vec{q}(t)$ as $|\vec{q}_{l_1}|$ to $|\vec{q}_{l_{\bar{k}}}|$, individually computed for each reference.

If $\exists\, p : |\vec{q}_{l_k}| \gg |\vec{q}_{l_j}|$, $\forall j \in \left\{1, \ldots, \bar{k}\right\}$, $j \neq k$, assume that solely reference R_{l_k} determines reset times and weights. If so, all other references are handled by the BLS and can be merged with the nonlinear RC response for R_{l_k} through superposition. This allows modelling of multi-sine Refs. [34].

This framework extends to permitting disturbances, as any sinusoidal disturbance $\vec{d}$ after the nonlinear reset element gives, for a linear plant, some sinusoidal signal $\vec{q}_d$. This can be handled analogous to $\vec{q}_{l_j}$ as described above.

7. Setup

The implications of the various assumptions are investigated in this section, evaluating where they cause δ-CL to not predict $\vec{e}(t)$ correctly. First, a precision positioning system will be introduced in this section. Afterwards, performance metrics are defined. For analysis $n = 1000$ harmonics are used. Series over impulse responses as in (32), (33) are evaluated with sufficient terms to ensure convergence.

7.1. Precision positioning stage

The 1 Degree-of-Freedom precision positioning stage depicted in Fig. 7 is used to validate the derived method. This SISO stage is a classic mass–spring–damper system. The transfer function of this stage is identified to be:

$$P(s) = \frac{3.038 \times 10^4}{s^2 + 0.7413\, s + 243.3} \tag{42}$$

The corresponding Bode Plot is given in Fig. 8. For the sake of analysis consider the simple case where (i) there is no noise, (ii) there are no disturbances, (iii) no quantization effects are present and (iv) a continuous-time controller is used.

7.2. Controllers

A linear PID controller $C(s)$ is added between the reset element and the plant, such that $G(s) = P(s)\,C(s)$. Parameter β is introduced, placing zero ω_d and pole ω_t symmetrically around bandwidth, defined as crossover frequency ω_c.

$$C(s) = k_p \left(\frac{s + \omega_i}{s}\right)\left(\frac{s + \omega_c\,/\,\beta}{s + \omega_c\,\beta}\right), \quad \beta = \frac{\omega_c}{\omega_d} = \frac{\omega_t}{\omega_c} \tag{43}$$

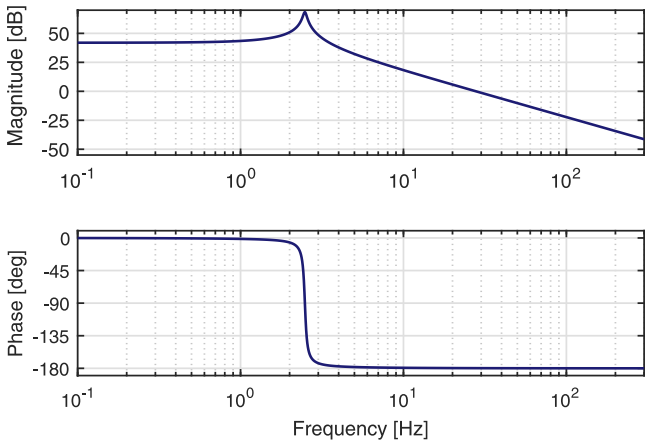

Fig. 8. Bode Plot corresponding to the system (42) shown in Fig. 7.

Table 2
Parameters for various CgLp and PID controller designs. For all $\mathcal{R}^\star$ controllers $\omega_i = 10$ Hz, $\omega_c = 100$ Hz and $\omega_f = 500$ Hz. Gain k_p is adjusted to achieve bandwidth ω_c.

	PM_{BLS}	ϕ_{RC}	γ	ω_r [Hz]	α	β
$\mathcal{R}_0^\star$	30°	20°	0	98.38	1.07	2.67
$\mathcal{R}_1^\star$	30°	20°	0.5	23.08	1.04	2.57
$\mathcal{R}_2^\star$	20°	20°	0.5	23.08	1.04	2.03

Bandwidth ω_c defined as the gain cross-over frequency is set to 100 Hz. Gain k_p is adjusted to achieve this bandwidth, based on DF analysis. For all implementations, $\omega_i = 10$ Hz is chosen.

Various CgLp-PID controller combinations tuned for different specifications are used for validation. Table 2 provides the corresponding tuning parameters. PM_{BLS} denotes the BLS phase margin. Let PM_{DF} be the phase margin as predicted by DF analysis. Then, the phase added through RC is given by $\phi_{RC} = PM_{DF} - PM_{BLS}$.

7.3. Performance metrics

The signal $\vec{e}(t)$ as predicted by (34) is compared to the corresponding simulated signal. A metric often used in literature for capturing the time-domain prediction accuracy is Integral Square Error (ISE). A normalized version is given by:

$$ISE(\omega) \triangleq \frac{\int \vec{e}_\omega(t) - \hat{\vec{e}}_\omega(t)^2 \, \mathrm{d}t}{\int \hat{\vec{e}}_\omega^2(t) \, \mathrm{d}t} \tag{44}$$

where simulation data is denoted by $\vec{e}$ and prediction data by $\hat{\vec{e}}$. A time vector with parameter ω, such as $\vec{e}_\omega(t)$, denotes the time response for a reference with frequency ω. In the high-tech industry peak error values indicate precision, described by the $\mathcal{L}_\infty$ norm, which is normalized:

$$L_\infty(\omega) \triangleq \frac{|\max_t |\vec{e}_\omega(t)| - \max_t |\hat{\vec{e}}_\omega(t)||}{\max_t |\hat{\vec{e}}_\omega(t)|} \tag{45}$$

8. Validation

Table 3 provides an overview of the various assumptions used by the three analytical RCS describing methods. CL-DF and δ-CL use similar assumptions, except for using different reset positions. This section will elaborate on the advantages of this modelling difference. Assumptions 2 and 3 of δ-CL are not mentioned in this section, because no results in this paper found Assumption 2 to not hold, whilst Assumption 3 is violated only for a few frequencies in one result, shown in Fig. 16. Assumption 5 is used to alleviate the constraint on having a sinusoidal $\vec{r}_l(t)$. This case will be demonstrated, after the effects of other assumptions on sensitivity prediction errors are verified using a sinusoidal input.

8.1. Effects of Assumption 1

Assumption 1 simplifies analysis by modelling two resets per period only, an assumption used by all analytical methods under consideration. However, this is known to invoke errors. A time domain example is provided to illustrate the types of errors inflicted. Then, it is shown how time regularization can decouple this error source from other sources.

Table 3
Overview of assumptions analytical methods for computing frequency-domain closed-loop RC behaviour use. Empty fields indicate that there are no assumptions. Note that assumptions on $\vec{r}_l$ do not have to cause errors, as $\vec{r}_l$ is designable.

	DF	CL-DF	δ-CL
Modelled resets per period:	2	2	2
Signals assumed sinusoidal:	$\vec{q}(t)$	$\vec{r}_l(t)$	$\vec{r}_l(t)$
Resets assumed at:		$\vec{q}_{DF,1} = 0$	$\vec{q}_{BLS} \approx 0$
Neglects harmonics:	Yes		

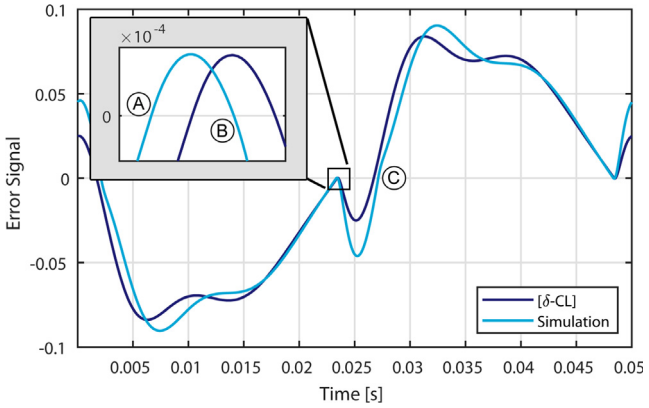

Fig. 9. Simulated and δ-CL predicted error response for a 20 Hz reference signal on controller $\mathcal{R}_1^\star$ and plant (42), thus using $\gamma = 0.5$. Points (A), (B) and (C) indicate reset instants. (B) is an undesired consecutive reset to (A), (C) is an additional reset.

Fig. 9 shows the simulated and δ-CL modelled error signals for a RCS generating three resets per half period, marked as (A), (B) and (C). Reset (A) is the one modelled by δ-CL, whereas (B) and (C) are not modelled, causing errors.

8.1.1. Consecutive resets

A pair of resets is said to be consecutive if they occur close together temporally, relative to period π / ω. Reset (B) in Fig. 9 is therefore consecutive to (A). Let the corresponding reset times be t_A and t_B, $t_B > t_A$. An ODE solution is used to express $\vec{x}(t_B)$ in terms of $\vec{x}(t_A^+)$:

$$\vec{x}(t_B) = e^{A_R(t_B - t_A)} x^+(t_A) + \int_{t_A}^{t_B} e^{A_R(t-\tau)} B_R \, u(\tau) \, \mathrm{d}\tau$$

Consider the limit case for consecutive resets, $t_B \to t_A$. Insert (1) to obtain $\vec{x}(t_B^+)$ as a function of $\vec{x}(t_A)$:

$$\lim_{t_B \to t_A} \vec{x}(t_B) = \vec{x}^+(t_A) = A_\rho \, \vec{x}(t_A)$$
$$\lim_{t_B \to t_A} \vec{x}^+(t_B) = A_\rho \, \vec{x}^+(t_A) \; = \; A_\rho^2 \, \vec{x}(t_A)$$

When comparing to (1) it follows that, for $t_{r,B} \to t_{r,A}$, the response becomes equivalent to that obtained by having one reset with reset matrix A_ρ^2. As all analytical methods model only one reset with reset matrix A_ρ, errors occur if $A_\rho \neq A_\rho^2$. For diagonal A_ρ parametrized by γ, such as in (8), modelling errors thus occur if $\gamma \neq \gamma^2 \Leftrightarrow \gamma \notin \{0, 1\}$. Full reset therefore does not invoke errors here. Fig. 9 uses $\gamma = 0.5$, meaning that the actual response to resets (A), (B) is almost equivalent to having one reset with $\gamma = 0.5^2 = 0.25$. This increases the reset-induced impulse weight (20), explaining the higher than modelled reset spike after (B).

8.1.2. Additional resets

Reset (C) in Fig. 9 is relatively far away from (A) in temporal sense. As such, $t_C \to t_A$ cannot be used here, implying that full reset is not exempt from errors caused by not modelling (C). Fig. 9 shows how (C) causes the error peak prediction to be wrong, inflicting L_∞ errors.

Fig. 10 gives ISE results for all three methods, plotted for a range of reference frequencies. Controllers $\mathcal{R}_0^\star$ ($\gamma = 0$) and $\mathcal{R}_1^\star$ ($\gamma = 0.5$) are used to control (42). Controller $\mathcal{R}_0^\star$ has, unlike $\mathcal{R}_1^\star$, negligible effects caused by consecutive resets because it is fully resetting. Both are affected by additional resets. Modelling errors of $\mathcal{R}_1^\star$ are, for all methods, at most frequencies, several factors above those of $\mathcal{R}_0^\star$, illustrating the considerable effects of consecutive resets on modelling accuracy. δ-CL is seen to invoke comparatively small prediction errors when consecutive resets do not affect the response ($\gamma = 0$).

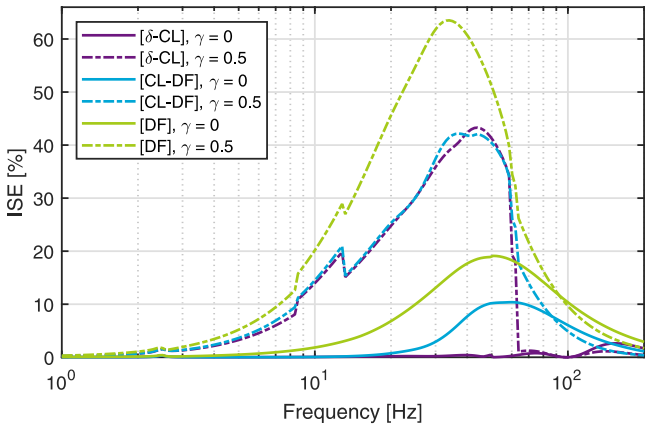

Fig. 10. Normalized ISE values for the three analytical modelling methods. No time regularization is used. Results are provided for controllers $\mathcal{R}_0^\star$ ($\gamma = 0$) and $\mathcal{R}_1^\star$ ($\gamma = 0.5$), both controlling plant (42).

8.1.3. Time regularization

Time regularization allows to remove consecutive or even additional resets, eliminating errors caused by Assumption 1. The following options are used:

- No time regularization: $\tau = 0$, such that all errors caused by consecutive and additional resets remain visible.
- Optimal time regularization: $\tau = 2\,\pi\,/\,(10\,\omega_c)$, ω_c in rad/s, suggested to be optimal when handling quantization [47]. This generally removes consecutive reset effects.
- Full time regularization: $\tau = \pi\,/\,\omega$, enforcing two resets per period, removing all errors caused by Assumption 1.

Full time regularization does not necessarily improve RC system performance. However, it decouples modelling error sources for δ-CL, as all remaining errors are caused by Assumption 4. This is employed to simplify analysis.

All three time regularization methods are applied to partially resetting controller $\mathcal{R}_1^\star$. Corresponding ISE results are given in Fig. 11. The DF and CL-DF descriptions show some improvement for more aggressive time regularization, but results are not consistent over all frequencies. δ-CL shows a significant performance improvement for more aggressive time regularization. In case of full time regularization, ISE values for δ-CL drop below 1.5%, errors that are thus solely caused by Assumption 4. ISE values for CL-DF with full time regularization are caused by the assumed reset positions and sinusoidal $\vec{q}(t)$, see Table 3. These two assumptions thus inflict considerably larger errors than Assumption 4 of δ-CL.

Example 8.1 (*CI Modelling*)**.** Potential errors caused by Assumption 1 are illustrated by means of a RCS with CI controller. Poor prediction performance is expected, as a CI often yields responses with many additional resets. Consider (42) with a fully resetting CI ($\gamma = 0$) in series with the following PD^2 controller:

$$C_{CI}(s) \;=\; k_p \left(\frac{s + \omega_c\,/\,\beta}{s + \omega_c\,\beta}\right)^2, \quad \beta = 3.73$$

where k_p is adjusted to ensure $\omega_c = 100$ Hz. This system has $PM_{BLS} = 30°$, with $\phi_{RC} = 51.9°$ added through CI [3]. The Bode plot is given in Fig. 12. As full reset is used, consecutive resets have negligible effects.

The ISE and L_∞ metrics are given for all three description methods by Fig. 13. ISE values in particular are found to be excessive, exceeding 100% for many frequencies, for all methods. This is explained by the time response for a 20 Hz reference, provided by Fig. 14. Without time regularization the simulated response is seen to have numerous resets per period, even affecting the weight of the modelled one.

For full time regularization the simulated response visually coincides with the δ-CL prediction. The marginal errors left must be caused by Assumption 4. The CL-DF erroneously predicts its reset time. This prediction is consistent with its $\vec{q}_{DF,1} = 0$ assumed reset time (see Table 3), but deviates considerably from the simulated signal.

8.2. Effects of Assumption 4

The effects of Assumption 4 can be isolated by applying full time regularization. $\Phi \ll 180°$ is assumed. Φ is expected to be small if the combined effects of all prior resets have dampened out at a reset instant. It follows that:

- More errors are expected at high frequencies, since there is less time between resets, thus less time for reset-induced impulses to dampen out.
- Higher errors are expected for a lower PM_{BLS}, as a lower PM generally increases settling times.

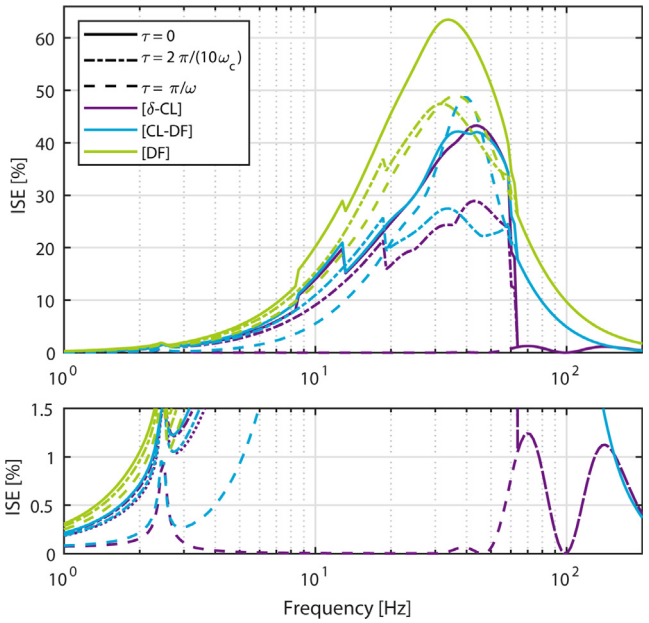

Fig. 11. Normalized ISE values for the three prediction methods, using controller $\mathcal{R}_1^\star$ on (42). Three different time regularization settings τ are used. The bottom figure provides a detail view on lower ISE values.

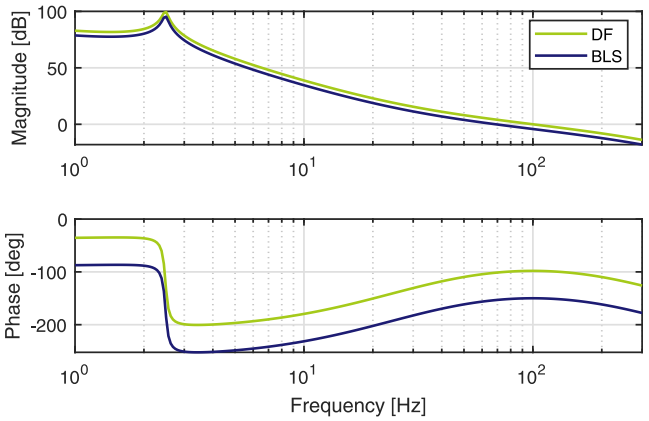

Fig. 12. Bode plot of (42) controlled by a CI and a linear controller C_{CI}. The BLS and first harmonic values as computed using DF analysis are given.

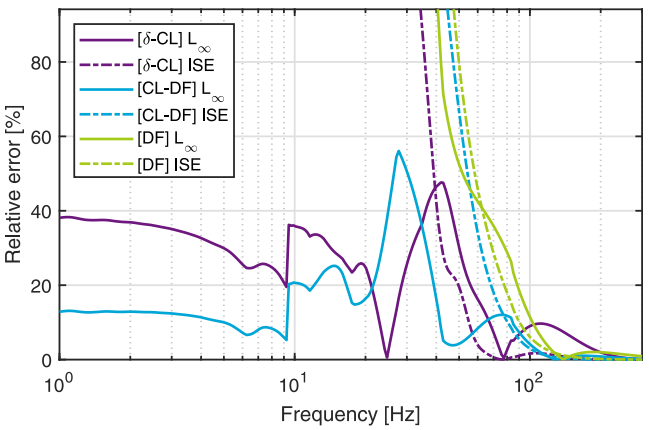

Fig. 13. ISE and L_∞ performance indicators for (42) controlled using a CI and C_{CI}. Results are shown for the three analytical describing methods.

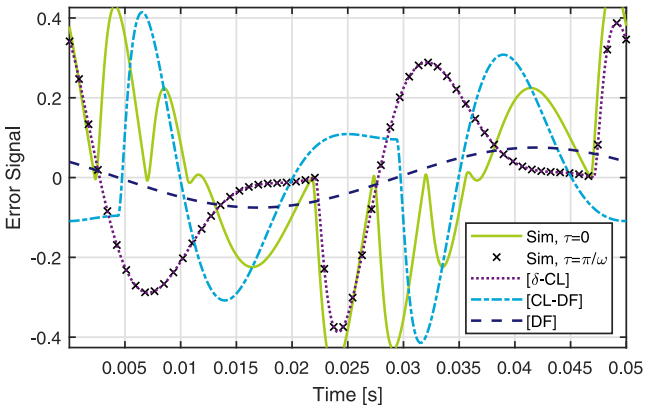

Fig. 14. Error time responses for (42) controlled using a CI and a linear controller C_{CI} with a 20 Hz unit magnitude reference. Simulated responses are given with either no ($\tau = 0$) or full ($\tau = \pi / \omega$) time regularization, in addition to modelled responses using the three analytical RC descriptions.

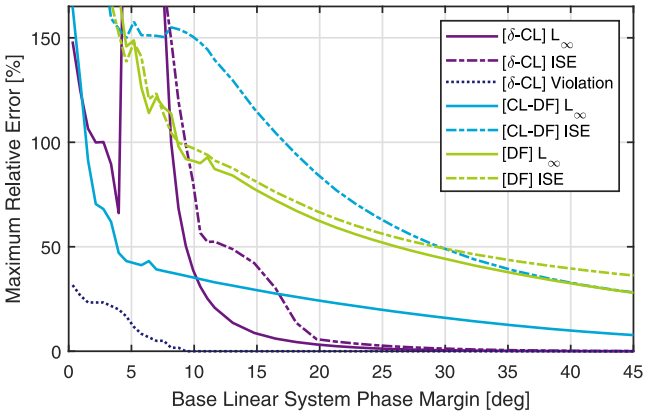

Fig. 15. Performance metrics plotted against PM_{BLS}, where the worst performing frequency between 10 and 100 Hz is used, per value of PM_{BLS}. The range of PM_{BLS} is obtained by sweeping β from 4.5 to 1.37, while otherwise using $\mathcal{R}_1^\star$ on (42). Full time regularization is used. The percentage of frequencies between 10 and 100 Hz violating Assumption 3 is given.

Fig. 15 gives the worst-case performance metrics when full time regularization is used, as a function of PM_{BLS}. Assumption 4 is found to be violated at very low values of PM_{BLS}. δ-CL will thus give erroneous results there. For reasonable PM_{BLS}, Fig. 15 shows that prediction errors due to Assumption 4 shrink when PM_{BLS} increases. At most PM_{BLS} points δ-CL greatly outperforms the DF and CL-DF descriptions, both in ISE and L_∞ terms. Fig. 16 provides ISE and Φ results for two controllers with different PM_{BLS} as function of frequency, using full time regularization. As such, all modelling errors are caused by Assumption 4, which means that the solutions should be exact if $\Phi = 0$. This holds, as can be seen in Fig. 16.

8.3. Effects of Assumption 5

This assumption extends the generality of δ-CL by permitting multi-sine references and disturbances. One of the worst cases for this assumption is if some other input has its peaks coinciding with the zero crossings of the base sinusoid, as this causes it to have a considerable effect on the reset times. Consider disturbance $\vec{d}$, introduced between $C(s)$ and $P(s)$, having a phase computed to meet this worst case scenario and magnitude parametrized by $\eta = |\vec{d}| \,/\, |\vec{r}_l|$. Fig. 17 gives sample predictions and simulations for various η.

The system without disturbance ($\eta = 0$) has a reset at (A), which is the one modelled by δ-CL. Assumption 5 considers the corresponding reference to be the only one causing resets. Predictions with disturbance therefore also model their resets at (A). However, the reset for $\eta = 0.1$ occurs at (B), causing a slight error in predicted peak position. The case for $\eta = 0.25$ is far worse, as it generates an additional reset at (C), which is not captured at all yet inflicts the largest error peak.

The effects of Assumption 5 depend on numerous parameters, including plant model, controller and input type. Its validity should therefore be evaluated per individual system.

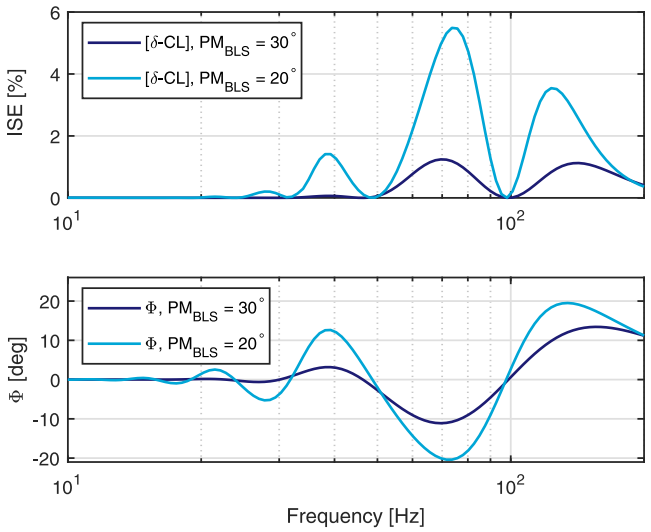

Fig. 16. ISE and Φ values, for $\mathcal{R}_1^\star$ and $\mathcal{R}_2^\star$ acting on (42), visualizing the relations between Φ, PM_{BLS} and ISE. Full time regularization is used.

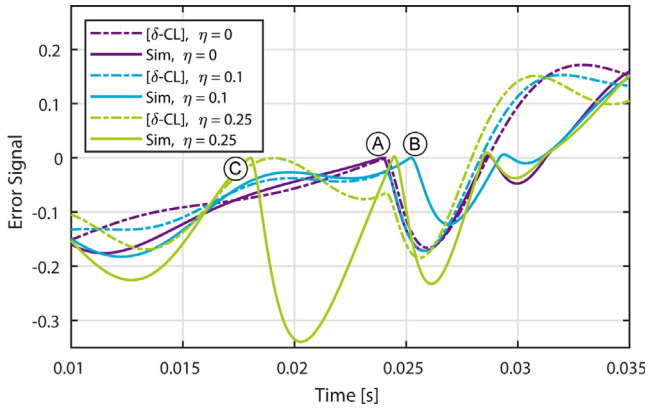

Fig. 17. Time domain simulations and δ-CL predictions for a 20 Hz reference and a 100 Hz disturbance with magnitudes η relative to the reference, using controller $\mathcal{R}_0^\star$ on (42). No time regularization is used. A half period response is shown. The disturbance phase is chosen such that its peaks coincide with zero-crossings of $\vec{q}(t)$ when there would not be a disturbance.

8.4. Method validity

The various error sources are found to be well-defined, as they can be clearly linked to Assumptions 1 or 4. In case both assumptions hold all modelling errors equal zero. As such the solution without assumptions, (28), is exact, which is as expected based on the mathematical derivation.

δ-CL is an approximation, relying on Assumptions 1 and 4. The former rarely holds in practice, yet does not necessarily inflict large errors, as additional resets are generally of lower magnitude than the modelled ones. Exceptions exist, as seen in Fig. 14 for $\tau = 0$. Increasing τ diminishes these errors.

Assumption 4 holds if PM_{BLS} is sufficiently large, in which case it inflicts small errors relative to Assumption 1. Based on Fig. 15, a $PM_{BLS} \gtrapprox 20°$ is advised for using δ-CL. These limits are system dependent.

9. Simulation results

The performance of δ-CL is further examined and compared to that of CL-DF and DF using various CgLp tunings, provided by Table 4. Optimal time regularization is used. Table 5 tabulates the peak and log-space average ISE and L_∞ metrics. From Table 5 it can be concluded that, in terms of ISE, δ-CL consistently outperforms CL-DF and DF. In terms of L_∞, differences between δ-CL and CL-DF are less pronounced, with either method yielding similar results, though both performing significantly better than DF. As expected, prediction errors increase when PM_{BLS} decreases. From comparing mean and median values for optimal and full time regularization it is concluded that the main error source for δ-CL must

Table 4
CgLp and PID controller details with ϕ_{RC} indicating the phase lead provided through reset at bandwidth as computed using DF analysis. For all controllers $\omega_i = 10$ Hz, $\omega_c = 100$ Hz and $\omega_f = 500$ Hz. Gain k_p is adjusted to achieve bandwidth ω_c.

	PM_{BLS}	ϕ_{RC}	γ	ω_r [Hz]	α	β
$\mathcal{R}_0$	20°	40°	0	34.41	1.24	2.17
$\mathcal{R}_1$	30°	30°	− 0.2	83.46	1.18	2.87
$\mathcal{R}_2$	30°	30°	0	62.88	1.15	2.78
$\mathcal{R}_3$	30°	30°	0.2	37.55	1.12	2.68
$\mathcal{R}_4$	40°	20°	0	98.38	1.07	3.59
$\mathcal{R}_5$	40°	30°	0	62.88	1.15	3.79
$\mathcal{R}_6$	50°	30°	0	62.88	1.15	5.79
$\mathcal{R}_7$	50°	40°	0	34.41	1.24	5.81

Table 5
Analytic RCS description method performance using plant (42) with the controllers in Table 4. Optimal time regularization is used. The relative peak and log-space average ISE and L_∞ results are given, evaluated between 1 Hz and bandwidth. Mean and median values are given for both optimal and full time regularization. All values provided are in percentage.

	$\max_\omega$ ISE			$\max_\omega L_\infty$			avg_ω ISE			$\text{avg}_\omega L_\infty$		
	δ-CL	CL-DF	DF	δ-CL	CL-DF	DF	δ-CL	CL-DF	DF	δ-CL	CL-DF	DF
Results for optimal time regularization:												
$\mathcal{R}_0$	69.0	94.0	114	33.1	19.0	94.1	12.5	16.1	23.6	5.30	4.35	22.6
$\mathcal{R}_1$	1.33	7.82	12.9	8.71	15.2	29.1	0.113	1.37	3.03	0.719	1.90	6.61
$\mathcal{R}_2$	2.63	11.0	16.8	7.22	10.7	31.1	0.383	1.93	4.13	1.20	1.78	7.62
$\mathcal{R}_3$	11.1	25.5	31.4	15.7	9.83	40.9	2.56	4.72	8.03	2.91	1.53	10.6
$\mathcal{R}_4$	0.0072	1.21	3.26	0.262	4.07	14.0	0.0012	0.215	0.791	0.0412	0.551	2.87
$\mathcal{R}_5$	1.63	7.77	12.6	5.94	5.55	22.6	0.287	1.59	3.34	0.963	1.13	6.02
$\mathcal{R}_6$	1.17	6.45	10.0	4.89	4.25	17.0	0.238	1.46	2.83	0.814	0.610	4.96
$\mathcal{R}_7$	12.9	38.0	40.0	13.7	5.62	30.2	3.26	10.5	12.3	3.32	1.37	10.2
mean:	12.5	24.0	30.1	11.2	9.28	34.9	2.38	4.74	7.26	1.91	1.65	8.94
median:	2.13	9.43	14.9	7.96	7.72	29.7	0.335	1.76	3.73	1.08	1.45	7.12
Results for full time regularization:												
mean:	2.65	48.7	42.0	2.62	20.4	47.8	0.181	7.28	8.63	0.220	3.12	10.6
median:	0.0358	13.6	17.0	0.620	14.6	36.8	0.00195	2.23	3.84	0.0438	2.34	7.30

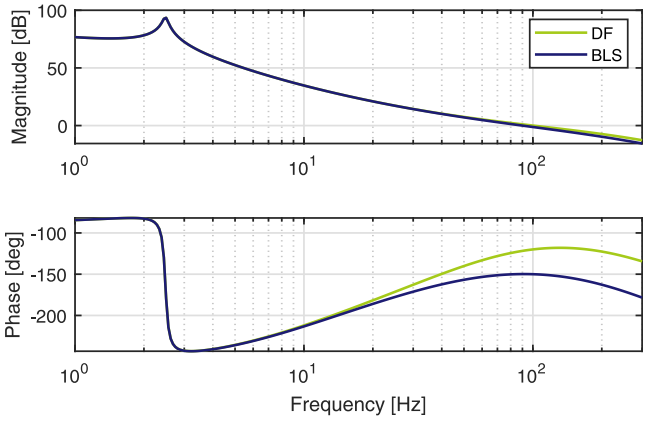

Fig. 18. Bode Plot for plant (42) with controller $\mathcal{R}_2$. The responses of the BLS and nonlinear RC modelled through DF analysis are shown.

be unmodelled resets, as prediction errors reduce significantly if full time regularization is applied. The same does not hold for CL-DF nor DF, which retain similar ISE and L_∞ values when removing additional resets.

9.1. Examining results for $\mathcal{R}_2$

Results for $\mathcal{R}_2$ are analysed in greater detail. This controller is selected because it roughly represents the median of all controllers in terms of performance. Fig. 18 provides the Bode plot for this setup, showing that the PM_{BLS} is 30° and that reset adds $\phi_{RC} = 30°$, as predicted through DF analysis.

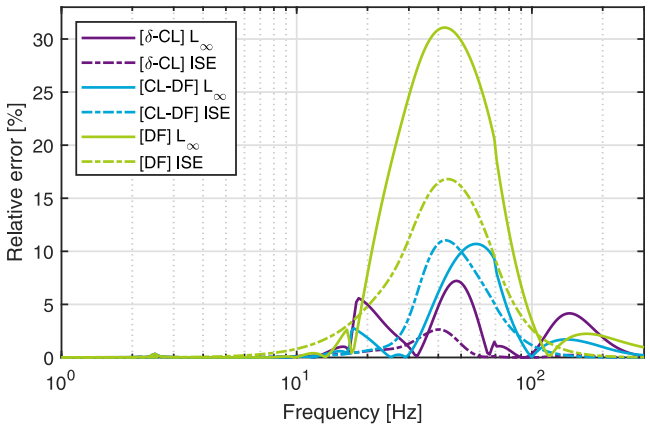

Fig. 19. L_∞ and ISE performance indicators for all three prediction methods over a range of frequencies, using plant (42) with controller $\mathcal{R}_2$. Optimal time regularization ($\tau = 2\pi/(10\omega_c)$) is used.

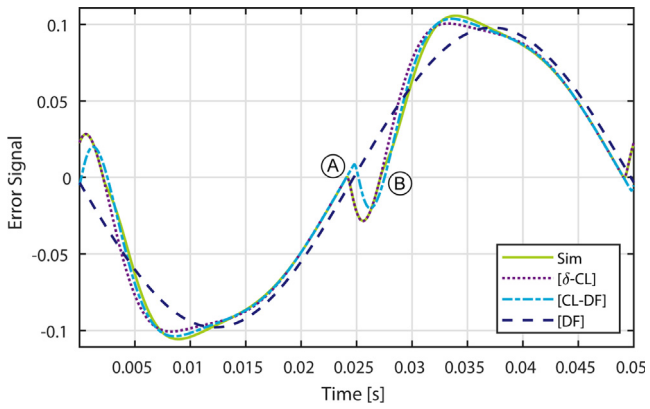

Fig. 20. Simulated and predicted error time responses for plant (42) with controller $\mathcal{R}_2$, using a 20 Hz sinusoidal $\vec{r}_l(t)$ with unit magnitude. The reset instants for a half period, (A) and (B), are indicated.

Fig. 19 shows the performance metrics for all three prediction methods. In terms of ISE, δ-CL outperforms CL-DF and DF. More subtle differences between δ-CL and CL-DF are found for the L_∞ metric, with either method improving upon the other in some frequency range. A time domain response is used for further analysis, given by Fig. 20 for a $\omega = 20$ Hz reference. At this frequency Fig. 19 indicates that, when considering L_∞, CL-DF outperforms δ-CL. The time domain responses show that δ-CL captures the effects of reset instant (A) accurately. Reset (B), considerably smaller in magnitude, is not modelled, causing the found ISE and L_∞ errors. Considering CL-DF, Fig. 20 shows that it models the response to (A) with some offset. While this causes ISE errors, this erroneous placement works to its advantage here, as the incorrect positioning of (A) compensates for not modelling (B) in evaluating the peak error, L_∞. As such, L_∞ performance of CL-DF is, in this case, better than that of δ-CL.

The erroneous impulse position prediction of CL-DF does not generally works to its advantage. Fig. 14 gives an example where large ISE errors are inflicted by the CL-DF reset placement assumption. Evaluating (19) shows that the error signal equals the BLS with added impulse responses. Thus, zero crossings occur near those of the BLS, provided that the impulse responses are sufficiently convergent. This supports that the reset placement assumption used by δ-CL is often more accurate than that of CL-DF.

10. Conclusion

Reset control can overcome fundamental limitations of linear control, whilst permitting design using the industry-preferred loop-shaping methodology. Even though accurate tuning through loop-shaping requires a thorough understanding of closed-loop behaviour, no frequency-domain methods found in literature sufficiently describe the principles of how open-loop reset control design translates to closed-loop behaviour. Additionally, no methods linking the base-linear system design to the closed-loop RCS performance is found.

A rarely mentioned approach, which models open-loop reset control as a linear system with state-dependent impulse train inputs, is taken and generalized. It is shown that any generic closed-loop reset system behaves as the base-linear system with added impulse responses. This describes, to the authors' knowledge, for the first time the underlying principles that link open-loop reset control design to its closed-loop performance, using frequency-domain terms as required for loop-shaping. This insight may be used to improve reset control design.

An analytical solution is obtained by inserting some well-defined assumptions. This description is critically examined using simulations and compared to existing methods. The novel description consistently provides a considerably more accurate time-domain prediction than the best performing analytical method found in literature, whilst having a similar performance in terms of predicted peak errors. It is shown how the various assumptions contribute to the prediction error, giving a good understanding of method limitations. High accuracy is attained if the base-linear system has sufficient phase margin and if unmodelled resets have a comparatively low magnitude, conditions met by various practical implementations.

Concluding, it is found that the presented description provides additional insight and improves predictions for reset control analysis, which can be used to improve reset element design. Further research should be conducted on how these results can be applied to practical reset control tuning.

CRediT authorship contribution statement

R.N. Buitenhuis: Conceptualization, Methodology, Software, Investigation, Validation, Writing – original draft. **N. Saikumar:** Conceptualization, Investigation, Supervision, Writing – review & editing. **S. Hassan HosseinNia:** Supervision, Writing – review & editing.

Declaration of competing interest

The authors declare that they have no known competing financial interests or personal relationships that could have appeared to influence the work reported in this paper.

Data availability

No data was used for the research described in the article.

Acknowledgments

This work was supported by the Dutch Research Council (NWO), through the Open Technology Program (OTP) Applied and Engineering Sciences (AES) Project, under Grant #16335.

References

[1] T. Samad, S. Mastellone, P. Goupil, A. van Delft, A. Serbezov, K. Brooks, IFAC industry committee update, initiative to increase industrial participation in the control community, IFAC Newslett. (2) (2019).
[2] H.W. Bode, Network Analysis and Feedback Amplifier Design, twelth ed., D. Van Nostrand Company, Inc, Princeton, New Jersy, 1945.
[3] J.C. Clegg, A nonlinear integrator for servomechanisms, Trans. Am. Inst. Electr. Eng. II: Appl. Ind. (ISSN: 0097-2185) 77 (1) (1958) 41–42, http://dx.doi.org/10.1109/tai.1958.6367399.
[4] A. Gelb, W.E. Vander Velde, Multiple-Input Describing Functions and Nonlinear System Design, first ed., McGraw-Hill Book Company, 1968.
[5] Isaac Horowitz, Patrick Rosenbaum, Non-linear design for cost of feedback reduction in systems with large parameter uncertainty, Internat. J. Control (ISSN: 13665820) 21 (6) (1975) 977–1001, http://dx.doi.org/10.1080/00207177508922051.
[6] Leroy Hazeleger, Marcel Heertjes, Henk Nijmeijer, Second-order reset elements for stage control design, in: Proceedings of the American Control Conference, Vol. 2016-July, (ISSN: 07431619) (2016) 2643–2648, http://dx.doi.org/10.1109/ACC.2016.7525315.
[7] Niranjan Saikumar, Hassan Hosseinnia, Microsystems Engineering, Generalized Fractional Order Reset Element (GFrORE), Vol. 2, Technical Report 1, Delft University of Technology, 2017.
[8] Nima Karbasizadeh, Ali Ahmadi Dastjerdi, Niranjan Saikumar, Duarte Valério, S. Hassan Hosseinnia, Benefiting from Linear Behaviour of a Nonlinear Reset-based Element at Certain Frequencies, Technical Report, Delft University of Technology, 2020.
[9] Orhan Beker, C.V. Hollot, Y. Chait, H. Han, Fundamental properties of reset control systems, IFAC Proc. Vol. (IFAC-PapersOnline) (ISSN: 14746670) 15 (1) (2004) 187–192, http://dx.doi.org/10.1016/j.automatica.2004.01.004,
[10] Yuqian Guo, Yuoyi Wang, Lihua Xie, Frequency-domain properties of reset systems with application in hard-disk-drive systems, IEEE Trans. Control Syst. Technol. (ISSN: 10636536) 17 (6) (2009) 1446–1453, http://dx.doi.org/10.1109/TCST.2008.2009066.
[11] Niranjan Saikumar, Rahul Kumar Sinha, S. Hassan HosseinNia, Resetting disturbance observers with application in compensation of bounded nonlinearities like hysteresis in piezo-actuators, Control Eng. Pract. (ISSN: 09670661) 82 (March 2018) (2019) 36–49, http://dx.doi.org/10.1016/j.conengprac.2018.09.026.
[12] Angel Vidal, Alfonso Baños, QFT-based design of PI+CI reset compensators: Application in process control, in: 2008 Mediterranean Conference on Control and Automation - Conference Proceedings, MED'08, 2008, pp. 806–811, http://dx.doi.org/10.1109/MED.2008.4602123.
[13] Angel Vidal, Alfonso Baños, Reset compensation for temperature control: Experimental application on heat exchangers, Chem. Eng. J. (ISSN: 13858947) 159 (1–3) (2010) 170–181, http://dx.doi.org/10.1016/j.cej.2010.02.033.
[14] D. Nešić, L. Zaccarian, A.R. Teel, Stability properties of reset systems, IFAC Proc. Vol. (IFAC-PapersOnline) (ISSN: 14746670) 38 (1) (2005) 67–72, http://dx.doi.org/10.3182/20050703-6-CZ-1902.00665,

[15] Francesco Fichera, Prieur Christophe, Sophie Tarbouriech, Luca Zaccarian, Using Luenberger observers and dwell-time logic for feedback hybrid loops in continuous-time control systems, Internat. J. Robust Nonlinear Control (ISSN: 10498923) 18 (October 2014) (2008) 557–569, http://dx.doi.org/10.1002/rnc, URL http://onlinelibrary.wiley.com/doi/10.1002/rnc.1553/abstract,
[16] Valiollah Ghaffari, Paknosh Karimaghaee, Alireza Khayatian, Reset law design based on robust model predictive strategy for uncertain systems, J. Process Control (ISSN: 09591524) 24 (1) (2014) 261–268, http://dx.doi.org/10.1016/j.jprocont.2013.11.017.
[17] Yuqian Guo, Youyi Wang, Lihua Xie, Hui Li, Weihua Gui, Optimal reset law design of reset control systems with application to HDD systems, in: Proceedings of the IEEE Conference on Decision and Control, IEEE, 2009, pp. 5287–5292, http://dx.doi.org/10.1109/CDC.2009.5399857, (ISSN: 01912216).
[18] Christophe Prieur, Sophie Tarbouriech, Luca Zaccarian, Lyapunov-based hybrid loops for stability and performance of continuous-time control systems, Automatica (ISSN: 00051098) 49 (2) (2013) 577–584, http://dx.doi.org/10.1016/j.automatica.2012.11.030.
[19] Leyao Li, Fen Wu, Xinmin Wang, A reset controller design method for MIMO linear systems, in: Chinese Control Conference, no. 2, CCC, TCCT, CAA, 2013, pp. 2132–2136, (ISSN: 21612927).
[20] S.J.L.M. van Loon, K.G.J. Gruntjens, M.F. Heertjes, N. van de Wouw, W.P.M.H. Heemels, Frequency-domain tools for stability analysis of reset control systems, Automatica (ISSN: 00051098) 82 (March) (2017) 101–108, http://dx.doi.org/10.1016/j.automatica.2017.04.008.
[21] W.H.T.M. Aangenent, G. Witvoet, W.P.M.H. Heemels, M.J.G. van de Molengraft, M. Steinbuch, Performance analysis of reset control systems, Internat. J. Robust Nonlinear Control 56 (26) (2009) http://dx.doi.org/10.1002/rnc.
[22] K.R. Krishnan, I.M. Horowitz, Synthesis of a non-linear feedback system with significant plant-ignorance for prescribed system tolerances, Internat. J. Control (ISSN: 13665820) 19 (4) (1974) 689–706, http://dx.doi.org/10.1080/00207177408932666.
[23] Y. Zheng, Y. Chait, C.V. Hollot, M. Steinbuch, M. Norg, Experimental demonstration of reset control design, Control Eng. Pract. (ISSN: 09670661) 8 (2) (2000) 113–120, http://dx.doi.org/10.1016/s0967-0661(99)00131-8.
[24] O. Beker, C.V. Hollot, Y. Chait, Plant with integrator: An example of reset control overcoming limitations of linear feedback, IEEE Trans. Automat. Control 46 (11) (2001) 1797–1799.
[25] Orhan Beker, Analysis of Reset Control Systems (Ph.D. thesis), University of Massachusetts, 2001.
[26] A. Feuer, G.C. Goodwin, M. Salgado, Potential benefits of hybrid control for linear time invariant plants, in: Proceedings of the American Control Conference, Vol. 5, 1997, pp. 2790–2794, http://dx.doi.org/10.1109/acc.1997.611964, (ISSN: 07431619).
[27] Erdi Akyüz, Niranjan Saikumar, S. Hassan Hosseinnia, Reset Control for Vibration Isolation, Technical Report, Delft University of Technology, 2019, URL https://repository.tudelft.nl/islandora/object/uuid:b627fe61-746a-4675-be57-cfc5808812ec.
[28] Alfonso Banos, Antonio Barreiro, Reset Control, first ed., Springer, London, ISBN: 1852338288, 2006, p. 221, http://dx.doi.org/10.1007/978-3-319-08413-8, URL http://scholar.google.com/scholar?hl=en&btnG=Search&q=intitle:Advances+in+Industrial+Control#0.
[29] Arun Palanikumar, Niranjan Saikumar, S. Hassan Hosseinnia, No more differentiator in PID: Development of nonlinear lead for precision mechatronics, in: 2018 European Control Conference, ECC 2018, 2018, pp. 991–996, http://dx.doi.org/10.23919/ECC.2018.8550088.
[30] Linda Chen, Niranjan Saikumar, Simone Baldi, S. Hassan Hosseinnia, Beyond the waterbed effect: Development of fractional order CRONE control with non-linear reset, in: Proceedings of the American Control Conference, Vol. 2018-June, 2018, pp. 545–552, http://dx.doi.org/10.23919/ACC.2018.8431572, (ISSN: 07431619).
[31] Linda Chen, Niranjan Saikumar, S. Hassan Hosseinnia, Senior Member, Development of robust fractional-order reset control, 2019, pp. 1–14.
[32] Niranjan Saikumar, Rahul Kumar Sinha, S. Hassan Hosseinnia, 'Constant in gain lead in phase' element-application in precision motion control, IEEE/ASME Trans. Mechatronics (ISSN: 10834435) 24 (3) (2019) 1176–1185, http://dx.doi.org/10.1109/TMECH.2019.2909082.
[33] Niranjan Saikumar, Duarte Val, S. Hassan Hosseinnia, Complex order control for improved loop-shaping in precision positioning, 2019, URL https://ieeexplore.ieee.org/document/9030150.
[34] Niranjan Saikumar, Kars Heinen, S. Hassan Hosseinnia, Loop-shaping for reset control systems: A higher-order sinusoidal-input describing functions approach, 2020, Delft University of Technology.
[35] Ali Ahmadi Dastjerdi, A. Astolfi, Niranjan Saikumar, N. Karbasizadeh, Duarte Valerio, S. Hassan HosseinNia, Closed-Loop Frequency Analyses of Reset Systems, Technical Report, Delft University of Technology, 2020, URL http://arxiv.org/abs/2001.10487.
[36] C.V. Hollot, Orhan Beker, Yossi Chait, Qian Chen, On Establishing Classic Performance Measures for Reset Control Systems, in: Perspectives in Ro- Bust Control, Lecture Notes in Control and Information Sciences, Springer - Verlag, New York, 2001, pp. 123–147.
[37] Yossi Chait, C.V. Hollot, On Horowitz's contributions to reset control, Internat. J. Robust Nonlinear Control (ISSN: 10498923) 12 (4) (2002) 335–355, http://dx.doi.org/10.1002/rnc.652.
[38] W.M. Haddad, V. Chellaboina, N.A. Kablar, Active control of combustion instabilities via hybrid resetting controllers, in: Proceedings of the American Control Conference, no. June, Chicago, (ISSN: 1883-8170) 2000, pp. 2378–2382, http://dx.doi.org/10.1002/9781119008972.ch4.
[39] Luca Zaccarian, Dragan Nešić, Andrew R. Teel, First order reset elements and the Clegg integrator revisited, in: Proceedings of the American Control Conference, Vol. 1, IEEE, ISBN: 0780390989, 2005, pp. 563–568, http://dx.doi.org/10.1109/ACC.2005.1470016, (ISSN: 07431619).
[40] M.F. Heertjes, K.G.J. Gruntjens, S.J.L.M. van Loon, N. van de Wouw, W.P.M.H. Heemels, Experimental evaluation of reset control for improved stage performance, IFAC-PapersOnLine (ISSN: 24058963) 49 (13) (2016) 93–98, http://dx.doi.org/10.1016/j.ifacol.2016.07.933.
[41] Yuqian Guo, Lihua Xie, Youyi Wang, Analysis and Design of Reset Control Systems, first ed., The Institution of Engineering and Technology, London, ISBN: 9781849197045, 2016, pp. 1–181, http://dx.doi.org/10.1049/PBCE094E.
[42] Kars Heinen, Frequency analysis of reset systems containing a Clegg integrator, 2018, Delft University of Technology, Delft, URL https://repository.tudelft.nl/islandora/object/uuid:ccc37af2-fcbc-46ec-9297-afdc5c1ea4b5.
[43] P.W.J.M. Nuij, O.H. Bosgra, M. Steinbuch, Higher-order sinusoidal input describing functions for the analysis of non-linear systems with harmonic responses, Mech. Syst. Signal Process. (ISSN: 08883270) 20 (8) (2006) 1883–1904, http://dx.doi.org/10.1016/j.ymssp.2005.04.006.
[44] V.S. Vladimirov, in: Alan Jeffrey (Ed.), Equations of Mathematial Physics, Marcel Dekker, Inc., New York, 1971, p. 81.
[45] D. Paesa, C. Franco, S. Llorente, G. Lopez-Nicolas, C. Sagues, Reset observers applied to MIMO systems, J. Process Control (ISSN: 09591524) 21 (4) (2011) 613–619, http://dx.doi.org/10.1016/j.jprocont.2010.12.011.
[46] Guanglei Zhao, Changchun Hua, Discrete-time MIMO reset controller and its application to networked control systems, IEEE Trans. Syst. Man Cybern.: Syst. (ISSN: 21682232) 48 (12) (2018) 2485–2495, http://dx.doi.org/10.1109/TSMC.2017.2707483.
[47] Bas Kieft, Niranjan Saikumar, S. Hassan Hosseinnia, Time Regularization as a Solution to Mitigate Quantization Induced Performance Degradation, Technical Report, Delft University of Technology, 2020, URL https://repository.tudelft.nl/islandora/object/uuid:db5f5a71-6212-4397-90b8-809701e31c9f?collection=education.